

Full length article



Thermal vibration analysis of cracked nanobeams submerged in elastic foundations by nonlocal continuum mechanics

Moustafa S. Taima^a, Tamer A. El-Sayed^{a,b,c,*}, Michael I. Friswell^d

^a Department of Mechanical Design, Faculty of Engineering, Mataria, Helwan University, P.O. Box 11718, Helmeiat-Elzaton, Cairo, Egypt

^b Centre for Applied Dynamics Research, School of Engineering, University of Aberdeen, Aberdeen, AB24 3UE, UK

^c School of Engineering, University of Hertfordshire Hosted by Global Academic Foundation, Cairo, Egypt

^d Faculty of Science and Engineering, Swansea University, Bay Campus, Fabian Way, Crymlyn Burrows, Swansea SA1 8EN, UK

ARTICLE INFO

Keywords:

Third-order shear deformation theory
Finite element method
Transverse vibration
Cracked nanobeam
Pasternak foundation
Thermal effect

ABSTRACT

Understanding the mechanical behavior of nanoscale structures is crucial in the development of advanced nanotechnologies. In this study, a novel approach to investigate the thermal lateral vibration of cracked nanobeams immersed in an elastic matrix is investigated. For this purpose, Reddy's third-order shear deformation theory (TSDT) is considered. In contrast to Timoshenko beam theory (First-order Shear Deformation Theory, FSDT), TSDT does not depend on a shear correction coefficient. The nano-scale effect is modeled using Eringen's nonlocal continuum mechanics theory. The nonlocal form of the governing equation is obtained through the application of Hamilton's principle. The weak form of the finite element global mass and stiffness matrices are obtained using Lagrange linear and Hermitian cubic interpolation. To model the crack in bending vibration, two rotational springs are used for TSDT, unlike the use of a single rotational spring in traditional Bernoulli–Euler (Classical Beam Theory, CBT) and FSDT. The stiffness of the springs is adjusted based on the severity of the crack. The influences of the nonlocal parameter, beam slenderness, position of crack, crack severity, Pasternak and Winkler foundation parameters, thermal effects and boundary conditions on the natural frequencies are investigated. The model's outcomes are compared with findings from prior publications, demonstrating a strong level of agreement. This study contributes to the growing research on nanostructures by presenting a novel approach to understanding the dynamics of cracked nanobeams using Reddy beam analysis-based solutions.

1. Introduction

Nanostructures have been proven to possess exceptional properties and have discovered a broad range of uses in fields such as thermal insulation, electronics, and micro/nano-electromechanical systems (MEMS/NEMS) [1], optoelectronics, microsurgery [2], drug delivery, cell manipulation [3] and etc. Gaining insight into the mechanical behavior of nanostructures is critical for developing an optimum design. Such understanding can be achieved either through experimentation or modeling. However, experimental investigation of nanoscale structures presents numerous challenges, as manipulating and measuring parameters at the nanometer scale is complex. Alternatively, modeling can be performed using either computer-based atomistic simulations or size-dependent nonlocal continuum mechanics. However, computer-based atomistic simulations, such as molecular dynamics, are computationally demanding and time-intensive [4]. The theory of nonlocal continuum

mechanics examines the mechanical behavior of nanostructures, encompassing aspects like bending, vibration, and buckling [5], offers a viable approach for studying these important objects at the nanoscale.

In the field of continuum mechanics, several nonlocal theories have been formulated to account for size-related effects. These include Eringen's nonlocal elasticity theory, the surface energy method, and the modified coupled stress theory [6,7]. These theories include additional terms in the governing equations that capture the interactions between material points over a finite distance and account for the size effect. Ceballes et al. [8] reviewed various nonclassical continuum mechanics theories, including differential nonlocal theory, Eringen's integral nonlocal theory, and general nonlocal theory. Eringen's strain-driven differential nonlocal elasticity theory is widely used because it can accurately model the size-dependent behavior of structures under different loading and boundary conditions. Eringen's hypothesis states that stress at a location results from strain throughout the continuum

* Corresponding author at: Centre for Applied Dynamics Research, School of Engineering, University of Aberdeen, Aberdeen, AB24 3UE, UK.

E-mail addresses: moustafa.samir@m-eng.helwan.edu.eg (M.S. Taima), tamer.el-sayed@abd.ac.uk (T.A. El-Sayed), m.i.friswell@swansea.ac.uk (M.I. Friswell).

<https://doi.org/10.1016/j.tws.2023.111249>

Received 3 August 2023; Received in revised form 22 September 2023; Accepted 2 October 2023

Available online 5 October 2023

0263-8231/© 2023 The Author(s). Published by Elsevier Ltd. This is an open access article under the CC BY license (<http://creativecommons.org/licenses/by/4.0/>).

Nomenclature

a	Internal characteristic length or crack depth
A	Beam cross-sectional area
b	Rectangular beam width
C_{ijkl}	Elastic modulus tensor
\mathbf{d}	Mode shape vector
e_0	Calibration parameter
$e^{i\omega t}$	Time term where, $i = \sqrt{-1}$
E	Young's modulus
G	Shear modulus
h	Rectangular beam height
H_i	Hermite cubic interpolation function
I	Second moment of area
k^*	Crack severity
k_p	Dimensionless Pasternak stiffness
k_w	Dimensionless Winkler stiffness
K^{eq}	Equivalent crack stiffness
K_p	Pasternak's stiffness parameter
K_w	Winkler's stiffness parameter
K_E	Kinetic energy
\mathbf{K}	Global stiffness matrix
\mathbf{K}_c	Crack stiffness matrix
\mathbf{K}_e	Reddy element stiffness matrix
l	External characteristic length
l_c	L_c/L crack location ratio
L	Total length of the beam
L_c	Crack location from left
L_i	Linear Lagrange interpolation function
θ	Pure bending slope $= -\partial w/\partial x$
κ	Shear correction factor
λ	Aspect or slenderness ratio $= L/h$
μ	$= (e_0 a)^2 = (\zeta L)^2$
ν	Poisson's ratio
ξ	Crack depth to height ratio $= a/h$
ρ	Density of the beam material
σ_{xx}	Normal stress
σ_{ij}	Stress tensor
M	Resultant general bending moment stress
M_b	Resultant pure bending moment stress
\mathbf{M}	Global mass matrix
\mathbf{M}_e	Element mass matrix
N	Resultant normal force stress
P_{th}	Axial thermal load
P_E	Potential energy
p_{th}	Thermal parameter
Q	Resultant shear force stress
t	Time
$u(x, t)$	Axial displacement
$v(x, t)$	Transverse displacement along y axis
$w(x, t)$	Transverse displacement along z axis
W_E	Work done by external loads
x	Reference point
x'	Any point in the body
α	Thermal expansion coefficient
α_0	Nonlocal Kernel function
γ_{xz}	Shear strain

δ	Variational symbol
Δ_e	Nodal value vector
ΔT	Temperature change
ϵ_{xx}	Normal strain
ϵ_{kl}	Strain tensor
ϵ_{th}	Thermal strain
ϵ_m	Mechanical strain
ζ	Nonlocal parameter $= (e_0 a)/l$
σ_{ij}^c	Classical stress tensor
τ_{xz}	Shear stress
φ_{av}	Average slope value
ψ	The slope at $z = 0$
ω	Natural frequency
$\bar{\omega}$	Dimensionless natural frequency
$\hat{\omega}$	$= \omega_{cracked} / \omega_{uncracked}$
Ω	Natural frequency in Hz
∇^2	Second order spatial gradient

around it and not simply at the place under consideration and also, allows for the inclusion of small-scale effects and interatomic forces as material parameters in the constitutive equations [9]. This model has been applied to study wave propagation, vibration, bending, buckling, and crack or impurity modeling of structures of different sizes, such as beams, shells, cones, plates, and graphene sheets [10–16]. The differential model has several advantages over other nonlocal elasticity models, including its simplicity, ease of implementation, and accuracy in capturing the behavior of structures with complex geometries and boundary conditions [17–19].

However, a paradox has emerged between Eringen's nonlocal elasticity integral and differential formulations, where some researchers have discovered a stiffening effect that arises from nonlocal interactions under certain boundary and loading conditions [20–22]. Proposed solutions to the paradox include using finite element methods, iterative techniques, Laplace transform methods, and the weighted residual approach to derive boundary conditions that are consistent with variations. Nevertheless, the presence of a paradox signals an ill-posed formulated elastostatic problem, wherein the stress field resulting from convolution fails to satisfy equilibrium conditions. Consequently, the choice of an appropriate theory should hinge upon the material's structure and its inherent properties. Moreover, certain higher-order theories within nonclassical continuum mechanics have not been implemented in physical systems because of the challenges involved in determining natural boundary conditions and interpreting the newly introduced parameters [22].

Yin et al. [6] presented an isogeometric analysis approach for size-dependent Euler–Bernoulli beams that satisfies the continuity requirement at the boundary conditions. Lignola et al. [23] used a closed-form analytical solution to present a well-posed analytical framework for the problem of a Timoshenko beam in an elastic medium. By applying constitutive boundary conditions, the integral form of the constitutive equation can be transformed into an equivalent differential equation [22,24].

Recently, Romano and Barretta introduced a stress-driven integral model, in which they showed that the new model is capable of generating a well-posed nonlocal elastic problem [25,26]. For the purpose of obtaining solutions to nonlocal problems, the differential form of nonlocal elasticity is generally preferred, but the integral form of nonlocal elasticity is a better choice for analyzing cantilever conditions than the differential model because it does not exhibit paradoxical behavior [19,23].

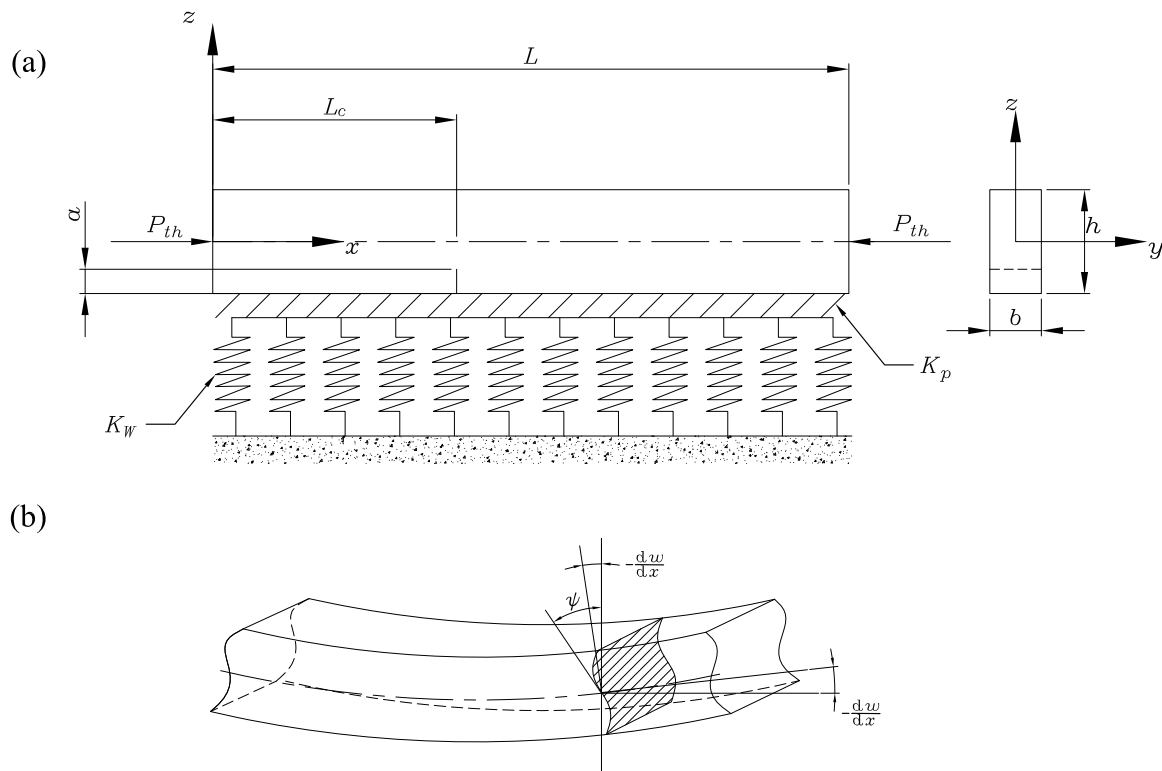


Fig. 1. (a) Cracked Reddy nanobeam under axial thermal load supported on a Winkler–Pasternak foundation. (b) Reddy beam parabolic shear strain and stress distribution.

To characterize the dynamical behavior of beams, several theories have been developed, including the Reddy, Levinson, Timoshenko, Rayleigh, and Bernoulli–Euler theories [21]. There are limitations to each of these theories. The most fundamental and well-established theory is the Bernoulli–Euler beam theory, which continues to be extensively used for slender beams, see for example [11,27,28]. Transverse shear deformation is not included in this theory. Timoshenko was the pioneer in emphasizing the importance of shear deformations in elastic beams [29]. Hence, Timoshenko beam theory is frequently utilized for the study of thick beams, see for example [30–37]. The assumption that the distribution of shear along the beam segment is roughly uniform is a limitation of this theory. This issue is corrected using the shear correction coefficient. The creation of higher-order theories (HSDTs) was prompted by the Timoshenko beam theory's limitations. One of the well-known HSDTs is the Reddy beam theory or (TSDT). It is assumed that the shear strain and stress in the transverse direction are distributed parabolically across the thickness of the beam in TSDT, as shown in Fig. 1(b). Unlike the Timoshenko theory, the TSDT does not require a shear coefficient κ [29].

In the past decade, some researchers have studied nanobeams modeled using TSDT in the literature. Reddy [13] and Aydogdu [14] examined the impact of nonlocal effects on the buckling, bending, and vibration of nanobeams. For each of the beam theories, such as Bernoulli–Euler, Timoshenko, Reddy, or Levinson, the authors employed Eringen's theory. For functionally graded micro/nano beams Salamat-Talab et al. [38] proposed the modified couple stress theory with TSDT. Lin and Xiang [39] studied the vibration of reinforced composite carbon nanobeams based on Timoshenko and TSDTs theories. Ansari et al. [40] presented the nonlinear dynamics of magneto-electro-thermo-elastic nanobeams under forced vibrations based on TSDT in conjunction with nonlocal elasticity theory.

In accordance with the third order shear deformation theory and Eringen's theory, Ebrahimi and Barati [41] researched the free vibration of functionally graded nanobeams. Mechab et al. [15] investigated the vibration of nanocomposite beams using higher order shear, while

taking nonlocal elasticity and Poisson's effect into account. Timoshenko and third-order shear deformation theory with the influence of surface stress were used by Lin et al. [42] to analyze the vibration and buckling behavior of nanobeams.

The behavior of NEMS/MEMS structures is strongly influenced by their atomic-scale features, and even small changes in the arrangement of atoms can have a significant impact on their response. Numerous studies have explored the fracture characteristics of carbon nanotubes, revealing that imperfections, such as missing atoms, can have a profound impact on the nanotube's strength, leading to the formation of cracks and eventual failure [43,44]. These cracked nanobeams are a crucial consideration in the design and construction of NEMS/MEMS structures because they can significantly impact the mechanical properties and overall performance of the structure. Thus, comprehending the behavior of cracked nanobeams is essential to the development of robust and dependable NEMS/MEMS devices.

Various techniques are available for modeling cracks, each with its own set of advantages and disadvantages. Examples include the spring model [44,45], reduction in cross section [46], and phase field [47–50]. In the spring model, which is used in the present work, the crack is modeled as a rotational spring. The stiffness of this spring fluctuates based on the intensity of the crack. The phase field model characterizes the crack as a diffuse area with a gradual gradient of material properties. The Reduction in cross section model reduces the cross-sectional area in the region where the crack is present, which accounts for the reduction in stiffness of the beam or shaft that results from the crack's presence. Nazemnezhad and Fahimi [51] presented free torsional vibration of nanobeams with a circumferential crack incorporating surface energy effects. According to the modified couple stress theory, Akbaş [52] studied the forced vibration of a cracked nano Timoshenko cantilever beam with damping. Using a finite element model, Aria et al. [16] investigated the lateral vibration of cracked Bernoulli–Euler nanobeams located in thermal environment. The beam was embedded on nonlocal elastic media with two parameters. Akbaş et al. [53] applied the finite element method and adapted

coupling stress theory to demonstrate the free vibration of cracked Bernoulli–Euler microbeams.

There are several approaches to approximately model the effect of elastic media such as Pasternak and Winkler foundations. Winkler’s model describes the elastic medium as a linear elastic spring system made up of dense independent linear springs [23,54]. According to the Winkler model, deformation only happens in the area where the load is applied. Loya et al. [55] studied the dynamic behavior of Timoshenko beams with cracks, which are embedded in a Winkler foundation. They modeled the crack using two massless extensional and rotational springs. Another model that is used to illustrate an elastic media is the Pasternak model. By fastening the spring ends to a beam or plate that only receives transverse shear deformation, the existence of shear interaction among the spring elements is allowed.

Nanomechanical devices may have to operate at a range of temperatures. The vibration characteristics alter when the temperature varies, and the impact of temperature on the vibration captivated the interest of scientists studying small-scale materials [56–59]. The majority of the literature-based study focuses on the temperature effect as well as the vibrational behavior of nanostructures contained in elastic medium. Among them and based on Eringen’s theory and Bernoulli–Euler beam theory, Demir and Civalek [60] considered the vibration of a nanobeam embedded in an elastic matrix under the thermal influence.

From the previous literature, the importance of investigating the dynamics of nanobeams, whether intact or cracked, is clear. This study proposes a novel approach to investigate the thermal lateral vibration behavior of nanoscale cracked beams by utilizing Reddy beam theory, in contrast to the conventional approaches based on Classical Beam Theory (CBT) and First-order Shear Deformation Theory (FSDT). To account for the size effect of the nanostructure, a nonlocal elasticity theory proposed by Eringen is incorporated into the model. Moreover, a crack model, comprising two rotational springs with stiffness that varies based on the severity of the crack, is integrated into the Reddy beam element. The analysis investigates the effects of several parameters, including the nonlocal parameter, slenderness ratio, crack location and severity, Pasternak and Winkler foundation parameters, thermal effects, and boundary conditions, on the natural frequencies of the nanobeam. After this introduction, the theoretical model based on TSDT is presented in Section 2 and the crack model is also discussed. Section 3 presents the model findings and verifications. Finally, Section 4 presents the key findings and conclusions.

2. Theoretical model

The model employed in this study is for a beam with total length L along the axial coordinate x and a uniform cross-sectional area A with width b and thickness (height) h along coordinates y and z respectively. (u, v , and w) are the displacements along the (x, y , and z) coordinate directions respectively. The transverse through edge crack on the beam measures a in depth and is located L_c from the left. It is considered that this crack will always be open. A two-parameter elastic base supports the beam (Winkler–Pasternak). The Pasternak foundation’s shear modulus is indicated as K_p , whereas the Winkler foundation’s linear spring constant is denoted by K_w . The beam axial load resulted from thermal stress is denoted by P_{th} .

2.1. The local formulation of governing equations

According to TSDT, the displacement field is expressed as follows:

$$\begin{aligned}
 u(x, z, t) &= u_0 + \left(z - \frac{4}{3h^2}z^3\right)\psi - \frac{4}{3h^2}z^3\frac{\partial w_0}{\partial x}, \\
 v(x, z, t) &= 0, \\
 w(x, z, t) &= w_0,
 \end{aligned}
 \tag{1}$$

where ψ denotes the slope $\varphi = \frac{\partial u}{\partial z}$ at $z = 0$ of the deformed line as shown in Fig. 1(b). The slope is derives as:

$$\varphi = \frac{\partial u}{\partial z} = \psi - \frac{4}{h^2}z^2\left(\psi + \frac{\partial w_0}{\partial x}\right).
 \tag{2}$$

The slope’s average value across the range $z \in [-h/2, h/2]$ is given by

$$\varphi_{av} = \frac{\int_{-\frac{h}{2}}^{\frac{h}{2}}\varphi dz}{h} = \frac{\left[z\psi - \frac{4}{3h^2}z^3\left(\psi + \frac{\partial w_0}{\partial x}\right)\right]_{-\frac{h}{2}}^{\frac{h}{2}}}{h} = \frac{2}{3}\psi + \frac{1}{3}\frac{-\partial w_0}{\partial x}.
 \tag{3}$$

The non-zero strain and stress components are described as:

$$\epsilon_{xx} = \frac{\partial u}{\partial x} = \frac{\partial u_0}{\partial x} + \left(z - \frac{4}{3h^2}z^3\right)\frac{\partial \psi}{\partial x} - \frac{4}{3h^2}z^3\frac{\partial^2 w_0}{\partial x^2},
 \tag{4}$$

$$\gamma_{xz} = 2\epsilon_{xz} = \frac{\partial u}{\partial z} + \frac{\partial w}{\partial x} = \left(1 - \frac{4}{h^2}z^2\right)\left(\psi + \frac{\partial w_0}{\partial x}\right),$$

$$\sigma_{xx} = E\epsilon_{xx} = E\left(\frac{\partial u_0}{\partial x} + \left(z - \frac{4}{3h^2}z^3\right)\frac{\partial \psi}{\partial x} - \frac{4}{3h^2}z^3\frac{\partial^2 w_0}{\partial x^2}\right),
 \tag{5}$$

$$\tau_{xz} = G\gamma_{xz} = G\left(1 - \frac{4}{h^2}z^2\right)\left(\psi + \frac{\partial w_0}{\partial x}\right),$$

where the beam Young’s and shear moduli are E and G respectively.

In order to implement the nonlocal theory the following stress resultants should be introduced

$$\begin{aligned}
 N &= \int_A \sigma_{xx} dA = EA u'_0, \\
 M &= \int_A \left(z - \frac{4}{3h^2}z^3\right)\sigma_{xx} dA = EI\left(\frac{68}{105}\psi' - \frac{16}{105}w''_0\right), \\
 M_b &= \int_A -\frac{4}{3h^2}z^3\sigma_{xx} dA = EI\left(-\frac{16}{105}\psi' + \frac{1}{21}w''_0\right), \\
 Q &= \int_A \left(1 - \frac{4}{h^2}z^2\right)\tau_{xz} dA = \frac{8}{15}GA\left(\psi + u'_0\right),
 \end{aligned}
 \tag{6}$$

where the differentiation with respect to x is denoted by superscript $'$. $I = \frac{bh^3}{12}$ is the cross-section moment of inertia, $\int\left(z^2, \frac{z^4}{h^2}, \frac{z^6}{h^4}\right)dA = I\left(1, \frac{3}{20}, \frac{3}{112}\right)$ and $\int\left(1, \frac{z^2}{h^2}, \frac{z^4}{h^4}\right)dA = A\left(1, \frac{1}{12}, \frac{1}{80}\right)$.

To obtain the governing equation, Hamilton’s principle states that the conservative system’s total potential energy must have a first variation equal to zero in the (t_1, t_2) time range.

$$\delta \int_{t_1}^{t_2} (K_E - (P_E + W_E))dt = 0,
 \tag{7}$$

where K_E , P_E and W_E denote the kinetic energy, potential (strain) energy and work done by the external loads, respectively. The variation of the kinetic energy is defined as

$$\delta K_E = \rho \int_0^L \int_A (\dot{w} \delta(\dot{w}) + \dot{u} \delta(\dot{u})) dAdx,
 \tag{8}$$

where time differentiation is represented by the dot notation and ρ is the mass density of the beam material. Thus,

$$\begin{aligned}
 \delta K_E &= \rho \int_0^L \int_A \left[(\dot{w}_0 \delta(\dot{w}_0)) + (\dot{u}_0 \delta(\dot{u}_0)) \right. \\
 &\quad + \left(\left(z^2 - \frac{8}{3h^2}z^4 + \frac{16}{9h^4}z^6 \right) \dot{\psi} + \left(\frac{-4}{3h^2}z^4 + \frac{16}{9h^4}z^6 \right) \dot{w}'_0 \right) \delta(\dot{\psi}) \\
 &\quad \left. + \left(\left(\frac{-4}{3h^2}z^4 + \frac{16}{9h^4}z^6 \right) \dot{\psi} + \left(\frac{16}{9h^4}z^6 \right) \dot{w}'_0 \right) \delta(\dot{w}'_0) \right] dAdx.
 \end{aligned}
 \tag{9}$$

Simplifying Eq. (9) gives

$$\begin{aligned}
 \delta K_E &= \int_0^L \left[\rho A (\dot{w}_0 \delta(\dot{w}_0) + \dot{u}_0 \delta(\dot{u}_0)) + \right. \\
 &\quad \left. \rho I \left(\left(\frac{68}{105}\dot{\psi} - \frac{16}{105}\dot{w}'_0 \right) \delta(\dot{\psi}) + \left(\frac{-16}{105}\dot{\psi} + \frac{1}{21}\dot{w}'_0 \right) \delta(\dot{w}'_0) \right) \right] dx.
 \end{aligned}
 \tag{10}$$

The strain energy's P_E variation may be represented as

$$\delta(P_E) = \int_A \int_0^L (\sigma_{xx} \delta(\epsilon_{xx}) + \tau_{xz} \delta(\gamma_{xz})) dx dA, \tag{11}$$

simplifying Eq. (11) gives

$$\delta(P_E) = \int_0^L (N \delta(u'_0) + M \delta(\psi') + M_b \delta(w''_0) + Q \delta(\psi) + Q \delta(w'_0)) dx. \tag{12}$$

The variation of the virtual work due to the elastic foundation and thermal load is given by

$$\delta(W_E) = \int_0^L (q\delta(w_0) + P_{th} w'_0 \delta(w'_0)) dx. \tag{13}$$

The axial force resulting from constraining the thermal expansion P_{th} equals the restraining force but in the negative direction as follows

$$P_{th} = EA\epsilon_m = -EA\epsilon_{th}, \tag{14}$$

where ϵ_{th} is the thermal strain and ϵ_m is the mechanical strain. The thermal strain can be evaluated from

$$\epsilon_{th} = \alpha\Delta T, \tag{15}$$

where ΔT is the temperature change and α is the thermal expansion coefficient. Substituting Eqs. (14) and (15) into Eq. (13) results in

$$\delta(W_E) = \int_0^L [(K_p - EA\alpha\Delta T) w'_0 \delta(w'_0) + K_w w_0 \delta(w_0)] dx. \tag{16}$$

The following weak form is obtained by inserting Eqs. (10), (12) and (16) into Eq. (7) and conducting integration by parts.

$$\begin{aligned} \int_{I_1}^{I_2} \delta(K_E - (P_E + W_E)) dt &= \int_{I_1}^{I_2} \int_0^L \left[\rho A (-\ddot{u}_0 \delta(u_0) - \ddot{w}_0 \delta(w_0)) \right. \\ &+ \rho I \left(\left(-\frac{68}{105} \ddot{\psi} + \frac{16}{105} \ddot{w}'_0 \right) \delta(\psi) + \left(\frac{-16}{105} \ddot{\psi}' + \frac{1}{21} \ddot{w}''_0 \right) \delta(w_0) \right) \\ &+ \frac{\partial N}{\partial x} \delta(u_0) + \frac{\partial M}{\partial x} \delta(\psi) - \frac{\partial^2 M_b}{\partial x^2} \delta(w_0) - Q \delta(\psi) + \frac{\partial Q}{\partial x} \delta(w_0) \\ &+ \left. \left((K_p - EA\alpha\Delta T) w'_0 - K_w w_0 \right) \delta(w_0) \right] dx dt \\ &+ \int_{I_1}^{I_2} \left[\rho I \left(\frac{16}{105} \ddot{\psi} - \frac{1}{21} \ddot{w}'_0 \right) \delta(w_0) - N \delta(u_0) + M \delta(\psi) - M_b \delta(w'_0) \right. \\ &+ \left. \frac{\partial M_b}{\partial x} \delta(w_0) - Q \delta(w_0) - (K_p - EA\alpha\Delta T) w'_0 \delta(w_0) \right] \Big|_0^L dt. \end{aligned} \tag{17}$$

The Euler-Lagrange equations of motion are:

$$\frac{\partial N}{\partial x} = \rho A \ddot{u}_0, \tag{18}$$

$$\begin{aligned} \frac{\partial Q}{\partial x} - \frac{\partial^2 M_b}{\partial x^2} &= -(K_p - EA\alpha\Delta T) w'_0 + K_w w_0 + \rho A \ddot{w}_0 + \frac{16}{105} \rho I \ddot{\psi}' \\ &- \frac{1}{21} \rho I \ddot{w}''_0, \end{aligned} \tag{19}$$

$$\frac{\partial M}{\partial x} - Q = \frac{68}{105} \rho I \ddot{\psi} - \frac{16}{105} \rho I \ddot{w}'_0. \tag{20}$$

The classical boundary conditions for the Reddy beam require specifying one element from each of the two pairs, as outlined in Table 1.

2.2. Nonlocal constitutive relation

The study in this paper is based on the differential form of nonlocal elasticity theory, developed by Eringen [61], which is regarded as one of the most powerful non-local continuum theories. According to Eringen [24] the constitutive equation of linear, homogeneous, isotropic, and nonlocal elastic solid with zero body forces are given by

$$\sigma_{ij}(x) = \int_v \alpha_0(|x' - x|, \zeta) \sigma_{ij}^c(x') dv(x'), \tag{21}$$

where the classical stress tensor is σ_{ij}^c and the stress tensor is σ_{ij} . A reference point is represented by x , a nearby point is represented by x' , and the nonlocal kernel function is represented by $\alpha_0(|x' - x|, \zeta)$. Both the distance between the points x and x' and the nonlocal parameter $\zeta = \frac{e_0 a}{l}$ have an impact on the kernel function α_0 . The lengths of the internal and external characteristics are denoted by the parameters a and l , respectively. The findings of the nonlocal model are compared to those of the atomic model using the parameter e_0 . However, it is still unclear which values are better for the small scaling parameter e_0 . For this parameter, numerous scholars proposed a number of values, and it was discovered that these values had a significant amount of scatter [9].

Equation's (21) integral may be reduced to the following partial differential equation:

$$(1 - \zeta^2 l^2 \nabla^2) \sigma_{ij}(x) = \sigma_{ij}^c(x) = C_{ijkl} \epsilon_{kl}(x), \tag{22}$$

where ∇^2 symbolizes the second order spatial gradient, ϵ_{kl} stands for the strain tensor, and C_{ijkl} represents the elastic modulus tensor. However, it is worth noting that, the conversion of the nonlocal model's integral form to its differential form represents a paradox in the problem of beam bending as discussed by Fernandez-Saez et al. [21], Romano et al. [22] and Barretta et al. [62]. They demonstrated how this transformation indicated a link between the bending moment and its spatial derivative at the beam boundary conditions, and they proved that this relationship should be matched. This indicates that the integral form of the nonlocal problem should be used to verify the differential form solution that was found. For problem with displacement type boundary conditions, this is important where the second order differential equation's solution is the bending moment and the bending moment boundary conditions that should be fulfilled by the integration constants. Nevertheless, the integral form is not viable to model the local effects at the boundaries. Considering the fact that each method has its limitations, here the differential form of the equation is used.

The nonlocal constitutive relations for beams (1D structures) are given as:

$$\sigma_{xx} - \mu \frac{\partial^2 \sigma_{xx}}{\partial x^2} = E \epsilon_{xx}, \quad \tau_{xz} - \mu \frac{\partial^2 \tau_{xz}}{\partial x^2} = G \gamma_{xz} \quad \text{where } \mu = (e_0 a)^2. \tag{23}$$

The constitutive relations for Reddy beam theory are

$$\begin{aligned} N - \mu \frac{\partial^2 N}{\partial x^2} &= EA u'_0, \\ M - \mu \frac{\partial^2 M}{\partial x^2} &= EI \left(\frac{68}{105} \psi' - \frac{16}{105} w''_0 \right), \\ Q - \mu \frac{\partial^2 Q}{\partial x^2} &= \frac{8}{15} GA (\psi + w'_0), \\ M_b - \mu \frac{\partial^2 M_b}{\partial x^2} &= EI \left(-\frac{16}{105} \psi' + \frac{1}{21} w''_0 \right), \end{aligned} \tag{24}$$

Substituting $\frac{\partial N}{\partial x}$ from Eq. (18) into the first of Eq. (24) gives

$$N = EA u'_0 + \mu \left(\rho A \ddot{u}_0 \right). \tag{25}$$

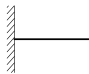
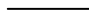
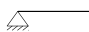
Substituting $\frac{\partial Q}{\partial x} - \frac{\partial^2 M_b}{\partial x^2}$ from Eq. (19) into the difference of the third and the first derivative of the fourth equations of Eq. (24) results in

$$\begin{aligned} \frac{\partial Q}{\partial x} - \frac{\partial^2 M_b}{\partial x^2} &= \frac{8}{15} GA (\psi' + w''_0) + EI \left(\frac{16}{105} \psi''' - \frac{1}{21} w_0'''' \right) \\ &+ \mu \left(-(K_p - EA\alpha\Delta T) w_0'''' + K_w w_0'' + \rho A \ddot{w}_0'' + \frac{16}{105} \rho I \ddot{\psi}''' - \frac{1}{21} \rho I \ddot{w}_0'''' \right). \end{aligned} \tag{26}$$

Using $\frac{\partial M}{\partial x} - Q$ from Eq. (20) and the difference of the first derivative of the second and third equations of Eq. (24) the following equation can be derived

$$\begin{aligned} \frac{\partial M}{\partial x} - Q &= EI \left(\frac{68}{105} \psi'' - \frac{16}{105} w_0''' \right) - \frac{8}{15} GA (\psi + w'_0) \\ &+ \mu \left(\frac{68}{105} \rho I \ddot{\psi}'' - \frac{16}{105} \rho I \ddot{w}_0''' \right). \end{aligned} \tag{27}$$

Table 1
Boundary conditions for Reddy beams.

		Displacement boundary conditions	Force boundary conditions
Clamped		$u_0 = 0$ $w_0 = 0$ $-\frac{\partial u_0}{\partial x} = 0$ $\psi = 0$	
Free			$N = 0$ $V = Q - \frac{\partial M_x}{\partial x} + (K_p - EA\alpha\Delta T) w'_0 - \frac{16}{105} \rho I \ddot{\psi} + \frac{1}{21} \rho I \dot{w}'_0 = 0$ $-M_b = 0$ $-M = 0$
Simply supported		$u_0 = 0$ $w_0 = 0$	$-M_b = 0$ $-M = 0$

The following equations of motion are provided after using Eqs. (18), (19) and (20) with Eqs. (25), (26) and (27).

$$EAu''_0 = \rho A(\ddot{u}_0 - \mu u''_0), \tag{28}$$

$$\begin{aligned} & \frac{8}{15} GA (\psi' + w''_0) + EI \left(\frac{16}{105} \psi''' - \frac{1}{21} w''''_0 \right) \\ & + (K_p - EA\alpha\Delta T) (w''_0 - \mu w''''_0) \\ & - K_w(w_0 - \mu w''_0) = \rho A(\ddot{w}_0 - \mu \ddot{w}''_0) + \frac{16}{105} \rho I(\ddot{\psi}' - \mu \ddot{\psi}''') \\ & - \frac{1}{21} \rho I(\ddot{w}''_0 - \mu \ddot{w}''''_0), \end{aligned} \tag{29}$$

$$\begin{aligned} & EI \left(\frac{68}{105} \psi'' - \frac{16}{105} w''''_0 \right) - \frac{8}{15} GA (\psi + w'_0) \\ & = \frac{68}{105} \rho I(\ddot{\psi} - \mu \ddot{\psi}'') - \frac{16}{105} \rho I(\ddot{w}'_0 - \mu \ddot{w}''''_0). \end{aligned} \tag{30}$$

The separation of variables concept is taken into account when solving these equations, by assuming that $u_0(x, t) = U(x)e^{i\omega t}$, $w_0(x, t) = W(x)e^{i\omega t}$ and $\psi(x, t) = \Psi(x)e^{i\omega t}$, where ω is the natural frequency. Substituting these relations into Eqs. (28), (29) and (30) results the following spatial equations

$$-EAU'' - \rho A\omega^2(U - \mu U'') = 0, \tag{31}$$

$$\begin{aligned} & \frac{-8}{15} GA (\Psi' + W''') - EI \left(\frac{16}{105} \Psi'''' - \frac{1}{21} W'''''' \right) \\ & - (K_p - EA\alpha\Delta T) (W'' - \mu W''''') \\ & + K_w(W - \mu W'') - \rho A\omega^2(W - \mu W'') - \frac{16}{105} \rho I\omega^2(\Psi' - \mu \Psi''') \\ & + \frac{1}{21} \rho I\omega^2(W'' - \mu W''''') = 0, \end{aligned} \tag{32}$$

$$\begin{aligned} & -EI \left(\frac{68}{105} \Psi'' - \frac{16}{105} W'''' \right) + \frac{8}{15} GA (\Psi + W') - \frac{68}{105} \rho I\omega^2(\Psi - \mu \Psi'') \\ & + \frac{16}{105} \rho I\omega^2(W' - \mu W''') = 0. \end{aligned} \tag{33}$$

The weak form of Eqs. (31), (32) and (33) over an element $(0, L)$ can be developed using arbitrary virtual displacements V , Y and Φ , where V is equivalent to the axial deflection U , Y is equivalent to the transverse deflection W , and Φ is equivalent to the rotation Ψ , i.e. $V \sim U$, $Y \sim W$, and $\Phi \sim \Psi$. After integration by parts (see Appendix A for further details), we obtain

$$\begin{aligned} 0 = & \int_0^L \left(EA V' U' - \rho A\omega^2 (VU + \mu V' U') \right) dx \\ & + \left[V (-EAU' + \mu \rho A\omega^2 U') \right]_0^L, \end{aligned} \tag{34}$$

$$\begin{aligned} 0 = & \int_0^L \left(\frac{8}{15} GA Y' (\Psi + W') - EI Y'' \left(\frac{16}{105} \Psi' - \frac{1}{21} W'' \right) \right. \\ & + (K_p - EA\alpha\Delta T) (Y' W' + \mu Y'' W'') + K_w (YW + \mu Y' W') \\ & - \rho A\omega^2 (YW + \mu Y' W') + \frac{16}{105} \rho I\omega^2 (Y' \Psi + \mu Y'' \Psi') \\ & \left. - \frac{1}{21} \rho I\omega^2 (Y' W' + \mu Y'' W'') \right) dx \\ & + \left[Y \left(\frac{-8}{15} GA (\Psi + W') - EI \left(\frac{16}{105} \Psi'' - \frac{1}{21} W'''' \right) \right. \right. \end{aligned} \tag{35}$$

$$\begin{aligned} & \left. - (K_p - EA\alpha\Delta T) (W' - \mu W''') \right. \\ & \left. - K_w (\mu W') + \rho A\omega^2 (\mu W') - \frac{16}{105} \rho I\omega^2 (\Psi - \mu \Psi'') \right. \\ & \left. + \frac{1}{21} \rho I\omega^2 (W' - \mu W''') \right) \\ & + Y' \left(EI \left(\frac{16}{105} \Psi' - \frac{1}{21} W'' \right) - (K_p - EA\alpha\Delta T) (\mu W'') \right. \\ & \left. - \frac{16}{105} \rho I\omega^2 (\mu \Psi') + \frac{1}{21} \rho I\omega^2 (\mu W''') \right) \Big|_0^L, \end{aligned}$$

$$\begin{aligned} 0 = & \int_0^L \left(EI\Phi' \left(\frac{68}{105} \Psi' - \frac{16}{105} W'' \right) + \frac{8}{15} GA\Phi (\Psi + W') \right. \\ & \left. - \frac{68}{105} \rho I\omega^2 (\Phi\Psi + \mu\Phi'\Psi') + \frac{16}{105} \rho I\omega^2 (\Phi W' + \mu\Phi' W'') \right) dx \\ & + \left[\Phi \left(-EI \left(\frac{68}{105} \Psi' - \frac{16}{105} W'' \right) + \frac{68}{105} \rho I\omega^2 (\mu \Psi') \right. \right. \\ & \left. \left. - \frac{16}{105} \rho I\omega^2 (\mu W''') \right) \right]_0^L. \end{aligned} \tag{36}$$

The nonlocal boundary conditions for Reddy beam can be obtained from Eqs. (34)–(36) in Table 2

According to Eq. (34) the axially displacement U must be differentiable at least once. Eqs. (35) and (36) demonstrate that, it is necessary for the rotation Ψ to be once differentiable and the transverse displacement W to be twice differentiable at least. For U and Ψ , linear Lagrange L_i functions are used, as well as Hermite cubic H_i interpolation functions for W , exact integration is used to get the element stiffness and mass matrices, which are presented in Appendix B. The displacements and rotation are approximated by:

$$U(x) = \sum_i^2 U_i V_i(x), \quad \Psi(x) = \sum_i^2 \Psi_i \Phi_i(x) \text{ and } W(x) = \sum_i^4 \Delta_i Y_i(x), \tag{37}$$

where Δ_i are given by:

$$\begin{aligned} \Delta_1 = [w]_{x=x_j}, \quad \Delta_2 = [\theta]_{x=x_j} = \left[-\frac{dw}{dx} \right]_{x=x_j}, \\ \Delta_3 = [w]_{x=x_{j+1}} \text{ and } \Delta_4 = [\theta]_{x=x_{j+1}} = \left[-\frac{dw}{dx} \right]_{x=x_{j+1}}, \end{aligned} \tag{38}$$

The j th element global nodal coordinates are (x_j, x_{j+1}) . Substituting Eq. (37) into Eqs. (34), (35) and (36) gives the finite element model Eq. (39) for free vibration analysis. The Reddy beam element has 8×8 mass and stiffness matrices, \mathbf{M}_e and \mathbf{K}_e with nodal generalized displacement vector $\mathbf{\Delta}_e = [U_1 \Delta_1 \Delta_2 \Psi_1 U_2 \Delta_3 \Delta_4 \Psi_2]^T$. Thus the local

Table 2
Nonlocal boundary conditions for Reddy beams.

Essential boundary conditions	Natural boundary conditions
$u_0 = 0$	$N = EAu'_0 + \mu\rho A \ddot{u}'_0 = 0$
$w_0 = 0$	$V \equiv \frac{8}{15} GA (\psi + w'_0) - EI \left(-\frac{16}{105} \psi'' + \frac{1}{21} w'''_0\right) + (K_p - EA\alpha\Delta T) (w'_0 - \mu w''_0) - \frac{16}{105} \rho I (\ddot{\psi} - \mu \ddot{\psi}'') + \frac{1}{21} \rho I (\ddot{w}'_0 - \mu \ddot{w}''_0) + \mu (K_{\omega} w'_0 + \rho A \ddot{u}'_0) = 0$
$-\frac{dw_0}{dx} = 0$	$M_b = EI \left(-\frac{16}{105} \psi' + \frac{1}{21} w''_0\right) + (K_p - EA\alpha\Delta T) \mu w'_0 - \mu \rho I \left(\frac{16}{105} \ddot{\psi}' + \frac{1}{21} \ddot{w}''_0\right) = 0$
$\psi = 0$	$M = EI \left(\frac{68}{105} \psi' - \frac{16}{105} w''_0\right) + \mu \rho I \left(\frac{68}{105} \ddot{\psi}' - \frac{16}{105} \ddot{w}''_0\right) = 0$

element equation of motion is

$$(\mathbf{K}_e - \omega^2 \mathbf{M}_e) \Delta_e = \mathbf{f}_e \tag{39}$$

where \mathbf{f}_e is the external force on the element from the rest of the beam. In Appendix B, these element matrices are provided. The thermal transverse vibrations are examined in this work, and therefore Eqs. (32) and (33) will be considered. Then, only the transverse and rotation degrees of freedom will be considered which reduces the element matrix size from 8×8 to 6×6 .

2.3. The model used for the crack

The crack is often represented as massless rotational and longitudinal elastic springs at the crack node, leading to a substructure approach [16,63]. This method's primary benefit is the division of an overall nonlinear system into several systems with local stiffness in linear subsystems discontinuities. In the case of locally cracked beams, the spring stiffnesses may be estimated using fracture mechanics. The loss of a single or many atoms from the nanobeams' structure as a result of manufacturing errors leads to higher strain energy, which may be likened to a crack in the continuum. The crack stiffness of a nanobeam must be determined using either preliminary investigations or molecular dynamics modeling. Furthermore, the coupling flexibility between axial and rotational directions is assumed to be negligible, and hence only the spring associated with the moment M is considered. The transverse deflections at the right and left nodes are comparable, according to the continuity requirement at the crack position, and it is assumed that the lateral the beam's stiffness at the crack point has not altered. It is assumed that the crack depth a is connected to the crack rotary spring's overall equivalent stiffness by:

$$K^{eq} = \frac{EI}{L} \frac{1}{k^*} \tag{40}$$

where the crack severity in the case of local beams is measured by the dimensionless local compliance known as $k^* = \frac{h}{L} C(\xi)$. The dimensionless function $C(\xi)$ is given by [63]

$$C(\xi) = \frac{\xi (2 - \xi)}{0.9 (\xi - 1)^2} \tag{41}$$

The crack depth to height ratio is given by $\xi = \frac{a}{h}$. Eq. (40) determines the stiffness of the corresponding rotational spring K^{eq} at the location of the cracked node. The value of K^{eq} approaches infinity for uncracked nodes.

The crack related rotational spring moment at the node is assessed in this case using the value of φ_{av} determined by Eq. (3). The moment caused by a rotational spring K_r , may thus be split into two components denoted by ψ and θ as follows.

$$\theta = \frac{-dw}{dx}, \tag{42}$$

$$M = K_r \varphi_{av} = K_r \left(\frac{2}{3} \psi + \frac{1}{3} \theta\right) = K_{c\psi} \psi + K_{c\theta} \theta,$$

where $K_{c\psi} = \frac{2}{3} K_r$ and $K_{c\theta} = \frac{1}{3} K_r$ and the subscript c denotes the crack.

According to Fig. 2, two parallel rotational springs hold the cross sections of the Reddy beam together. The bending and rotation slopes at the left end of the element are θ^L and ψ^L , respectively. Also, the rotation and bending slopes at the right end of the element are ψ^R , and θ^R , respectively. w is the lateral displacement of the node. The

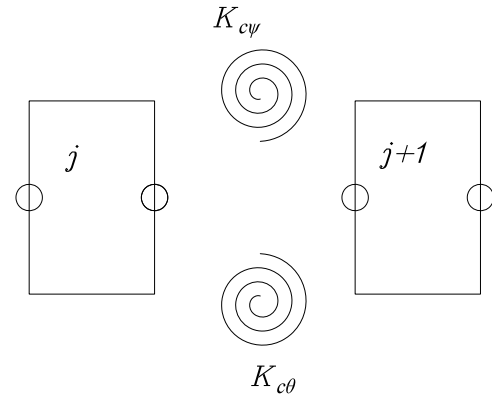


Fig. 2. The crack rotational spring model.

continuity criteria at the crack position imply that the lateral deflection at the right and left nodes is equal, i.e. $w^R = w^L$. The torsional stiffness links the rotations ψ^L , θ^L , and ψ^R , θ^R of these nodes. The crack's stiffness matrix may be derived in the form:

$$\mathbf{K}_c = \begin{bmatrix} K_{c\theta} & 0 & 0 & -K_{c\theta} & 0 \\ 0 & K_{c\psi} & 0 & 0 & -K_{c\psi} \\ 0 & 0 & 0 & 0 & 0 \\ -K_{c\theta} & 0 & 0 & K_{c\theta} & 0 \\ 0 & -K_{c\psi} & 0 & 0 & K_{c\psi} \end{bmatrix} \tag{43}$$

With the exception of the fractured zone, the conventional finite element method is used in the assembly process for the cracked beam. The two elements surrounding the crack are combined with the crack element as shown in Eq. (44). The left element to the crack will be reordered according to displacement vector $[w_1 \ \theta_1 \ \psi_1 \ \theta_2 \ \psi_2 \ w_2]$ and coupled to the crack matrix as shown in the matrix (see Eq. (44) given in Box I where K_{ij}^L and $K_{ij}^R(i, j = 1 : 6)$ are the stiffness matrices for left and right beam elements, which are assembled with the crack torsional springs with stiffnesses $K_{c\theta}$ and $K_{c\psi}$.

2.4. The overall mass and stiffness matrices

In the overall matrices, n cracks and N nodes combine to form a $(3N + 2n) \times (3N + 2n)$ matrix. The cracked beam is assembled using the traditional finite element technique except at the cracked region where the two elements surrounding the crack are replaced by the crack element which leads to evaluating the overall mass \mathbf{M} and stiffness \mathbf{K} matrices of a cracked Reddy beam.

2.5. Obtaining mode shapes and natural frequencies

In free vibration analysis of an undamped beam, mode shapes and the natural frequencies may be found using the overall mass \mathbf{M} and stiffness \mathbf{K} matrices. Typically, the undamped eigenvalues may be found by solving

$$[\mathbf{K} - \omega_i^2 \mathbf{M}] \mathbf{d}_i = 0, \tag{45}$$

where \mathbf{d}_i is the beam's matching mode shape vector and ω_i denotes the i th natural frequency. The natural frequencies and beam mode shapes were determined using MATLAB code.

$$\mathbf{K} = \begin{matrix} w_1 \\ \theta_1 \\ \psi_1 \\ \theta_2^L \\ \psi_2^L \\ w_2 \\ \theta_2^R \\ \psi_2^R \\ w_3 \\ \theta_3 \\ \psi_3 \end{matrix} \begin{bmatrix} K_{11}^L & K_{12}^L & K_{13}^L & K_{14}^L & K_{15}^L & K_{16}^L & 0 & 0 & 0 & 0 & 0 \\ K_{21}^L & K_{22}^L & K_{23}^L & K_{24}^L & K_{25}^L & K_{26}^L & 0 & 0 & 0 & 0 & 0 \\ K_{31}^L & K_{32}^L & K_{33}^L & K_{34}^L & K_{35}^L & K_{36}^L & 0 & 0 & 0 & 0 & 0 \\ K_{41}^L & K_{42}^L & K_{43}^L & K_{44}^L + K_{c\theta} & K_{45}^L & K_{46}^L & -K_{c\theta} & 0 & 0 & 0 & 0 \\ K_{51}^L & K_{52}^L & K_{53}^L & K_{54}^L & K_{55}^L + K_{c\psi} & K_{56}^L & 0 & -K_{c\psi} & 0 & 0 & 0 \\ K_{61}^L & K_{62}^L & K_{63}^L & K_{64}^L & K_{65}^L & K_{66}^L + K_{11}^R & K_{12}^R & K_{13}^R & K_{14}^R & K_{15}^R & K_{16}^R \\ 0 & 0 & 0 & -K_{c\theta} & 0 & K_{21}^R & K_{22}^R + K_{c\theta} & K_{23}^R & K_{24}^R & K_{25}^R & K_{26}^R \\ 0 & 0 & 0 & 0 & -K_{c\psi} & K_{31}^R & K_{32}^R & K_{33}^R + K_{c\psi} & K_{34}^R & K_{35}^R & K_{36}^R \\ 0 & 0 & 0 & 0 & 0 & K_{41}^R & K_{42}^R & K_{43}^R & K_{44}^R & K_{45}^R & K_{46}^R \\ 0 & 0 & 0 & 0 & 0 & K_{51}^R & K_{52}^R & K_{53}^R & K_{54}^R & K_{55}^R & K_{56}^R \\ 0 & 0 & 0 & 0 & 0 & K_{61}^R & K_{62}^R & K_{63}^R & K_{64}^R & K_{65}^R & K_{66}^R \end{bmatrix}, \quad (44)$$

Box I.

3. Results and discussion

The current section includes two subsections, the first of which validates the model using previously published literature. The second section presents and discusses new findings.

The dimensionless parameters utilized in this investigation are

$$\bar{\omega} = \left(\frac{\rho A}{EI} \omega^2 L^4 \right)^{\frac{1}{4}}, \quad \xi = \frac{a}{h}, \quad (46)$$

$$\xi = \frac{a}{h}, \quad (47)$$

$$k^* = \frac{h}{L} \frac{\xi (2 - \xi)}{0.9 (\xi - 1)^2} \quad (48)$$

$$l_c = \frac{L_c}{L}, \quad (49)$$

$$\lambda = \frac{L}{h}, \quad (50)$$

$$k_w = \frac{K_w L^4}{EI}, \quad (51)$$

$$k_p = \frac{K_p L^2}{EI}, \quad (52)$$

$$p_{th} = \frac{E \alpha \Delta T L^2}{EI}, \quad (53)$$

$$\hat{\omega} = \frac{\omega_{cracked}}{\omega_{uncracked}} \quad (54)$$

where, $\bar{\omega}$ refers to the dimensionless natural frequency, ξ is the crack depth ratio, k^* is the crack severity, l_c represents the crack position ratio, and λ denotes slenderness ratio. Additionally, p_{th} is the dimensionless temperature, k_p is Pasternak stiffness, and k_w refers to Winkler stiffness. The natural frequency in Hertz ($\Omega = \frac{\omega}{2\pi}$) and the frequency ratio of the cracked to uncracked state $\hat{\omega}$ are also defined. The results are obtained based on a numerical model consisting of 100 beam elements.

3.1. Validation

The current study includes many parameters that should be taken into consideration to ensure a thorough verification procedure. The various parameters are the aspect (or slenderness) ratio, crack location, crack depth or severity, nonlocal parameters, elastic foundation stiffness, temperature, and boundary conditions.

3.1.1. Convergence rate

Table 3 provides convergence rates, offering a comparative analysis between the present model at nonlocal $\zeta = \frac{e_0 a}{L} = 0$ against outcomes

derived from the classical 3D Finite Element Analysis (FEA) executed via ANSYS from Ref. [64]. Within Table 3, the natural frequencies Ω_i (Hz) are presented for both the intact beam ($\xi = 0$) and the cracked beam characterized by a depth ratio of $\xi = 0.4$. These analyses encompass two distinct crack location ratios, $l_c = 0.25$ and 0.5 , within a beam with a total length of $L = 0.4$ m, a slenderness ratio of $\lambda = 20$, and material properties denoted by $E = 216$ GPa, $\rho = 7850 \frac{kg}{m^3}$, and $\nu = 0.3$.

The results in Table 3 show rapid convergence in response to an increase in the number of elements (N_e). As N_e approaches 100, the level of accuracy attained within the results is deemed satisfactory. Therefore, this specific number of elements is selected. Furthermore, the inclusion of the percentage error demonstrates a strong agreement between the present model and 3D FE [64], as the error percentage remains consistently below 1.32%.

3.1.2. Effects of crack location ratio for normal size Reddy beam

A simply supported–simply supported (S-S) cracked beam’s first three natural frequencies are contrasted with those from Ref. [64] in Fig. 3. The natural frequencies results for a beam with crack depth ratios of $\xi = 0$ and 0.4 are plotted versus different crack location ratios l_c . The total length of beam is $L = 0.4$ m and a slenderness ratio $\lambda = 20$. The beam properties are $E = 216$ GPa, $\rho = 7850 \text{ kg/m}^3$, and $\nu = 0.3$. The results of Fig. 3 show that the present model results are coincident with that of TSDT in Ref. [64]. Also, the figure shows that the sensitivity of the natural frequencies change with the crack location and the vibration mode.

3.1.3. Thermal effect on an uncracked nonlocal beam

The dimensionless fundamental natural frequency $\bar{\omega}_1$ for a very thin clamped–clamped (C-C) beam is compared with that of [16,60] and the results are given in Table 4. The results are obtained for different temperature parameter (thermal load) p_{th} and nonlocal parameter $\zeta = \frac{e_0 a}{L}$. The results in Table 4 indicate that increasing the temperature or nonlocal parameters decreases the natural frequency. The findings of this investigation and those of Refs. [16,60] are in good agreement

3.1.4. Nonlocal parameter effect on beam embedded in an elastic Winkler and Pasternak foundation

The effects of the nonlocal parameter ζ for very thin S-S beams are compared with those from Ref. [16,60] in Table 5. The beam is embedded in an elastic foundation with stiffness parameters $k_w = 10$, $k_p = 5$. The results in Table 5 show the first four dimensionless frequencies $(\bar{\omega}_n)^2$, which indicate that the natural frequencies decrease as the nonlocal parameter is increased. The validation results indicate that the findings of this study and the relevant literature reference studies show a strong agreement.

Table 3
Convergence rate and error percentage (Er%) of the first three natural frequencies Ω_i (Hz).

Case	Ω_i (Hz)	N_e									3D FE [64]
		4	8	12	16	20	40	60	80	100	
Uncracked	1st	303.5	297.7	296.7	296.4	296.2	296.1	296.1	296.1	296.1	296.1
	Er %	2.5	0.54	0.2	0.09	0.04	-0.01	-0.01	-0.01	-0.01	
	2nd	1290.8	1196	1179.7	1174.5	1172.4	1170.1	1169.9	1169.8	1169.8	1170.4
$l_c = 0.25$	3rd	3153.7	2710.3	2629.6	2603.8	2593.2	2582.4	2581.2	2580.9	2580.8	2583.7
	Er %	22.06	4.9	1.78	0.78	0.37	-0.05	-0.1	-0.11	-0.11	
	1st	288.5	283.5	282.6	282.3	282.1	281.9	281.9	281.8	281.8	283.9
$l_c = 0.5$	Er %	1.63	-0.13	-0.46	-0.57	-0.62	-0.7	-0.72	-0.73	-0.74	
	2nd	1167	1095.6	1083.2	1079.1	1077.3	1075.2	1074.8	1074.5	1074.4	1086.8
	Er %	7.38	0.81	-0.33	-0.71	-0.87	-1.06	-1.1	-1.13	-1.14	
$l_c = 0.5$	3rd	3015.6	2606.5	2534.9	2511.9	2502.4	2492.5	2491.3	2490.9	2490.7	2502
	Er %	20.52	4.18	1.31	0.4	0.02	-0.38	-0.43	-0.45	-0.45	
	1st	275.9	271.4	270.6	270.3	270.1	269.9	269.8	269.7	269.7	273.3
$l_c = 0.5$	Er %	0.94	-0.68	-0.99	-1.1	-1.16	-1.25	-1.28	-1.31	-1.32	
	2nd	1290.8	1196	1179.7	1174.5	1172.4	1170.1	1169.9	1169.8	1169.8	1170.2
	Er %	10.31	2.2	0.81	0.37	0.18	-0.01	-0.03	-0.04	-0.04	
$l_c = 0.5$	3rd	2854.9	2490	2428.4	2408.6	2400.3	2391.4	2390	2389.5	2389.1	2411.3
	Er %	18.39	3.26	0.71	-0.11	-0.46	-0.83	-0.88	-0.91	-0.92	

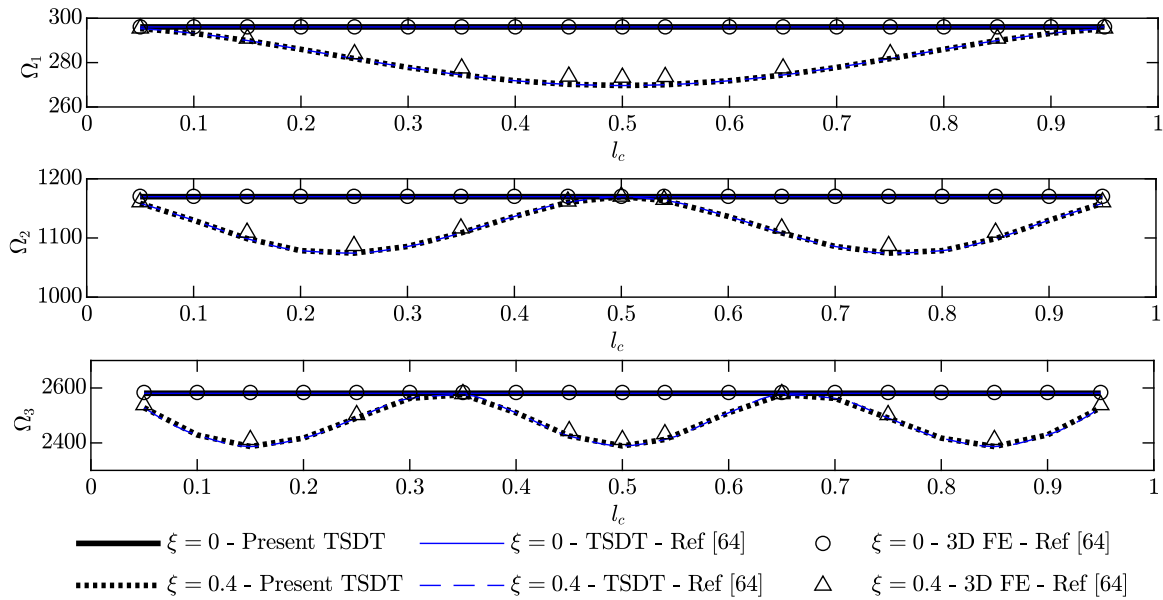


Fig. 3. (Color online) First three natural frequencies of a cracked beam Ω_i in Hertz with crack depth ratios $\xi = 0$ and 0.4 versus crack location ratio.

Table 4
The fundamental dimensionless natural frequency $\bar{\omega}_1$ for different temperature p_{th} and nonlocal $\zeta = \frac{e_0 a}{L}$ parameters.

p_{th}	$\zeta = \frac{e_0 a}{L} = 0$			$\zeta = \frac{e_0 a}{L} = 0.1$			$\zeta = \frac{e_0 a}{L} = 0.2$		
	a	b	c	a	b	c	a	b	c
-3	4.8148	4.8140	4.8134	4.7095	4.7087	4.7083	4.4712	4.4703	4.4701
-2	4.7871	4.7861	4.7857	4.6721	4.6713	4.6709	4.4092	4.4084	4.4081
-1	4.7588	4.7582	4.7575	4.6338	4.6330	4.6325	4.3444	4.3436	4.3433
0	4.7300	4.7292	4.7287	4.5945	4.5936	4.5931	4.2766	4.2759	4.2754
1	4.7007	4.6993	4.6993	4.5541	4.5532	4.5527	4.2054	4.2047	4.2041
2	4.6707	4.6696	4.6693	4.5125	4.5117	4.5111	4.1304	4.1296	4.1285
3	4.6402	4.6397	4.6387	4.4697	4.4689	4.4683	4.0510	4.0503	4.0499

a- Ref. [60], b- Ref. [16], c- Present results.

3.2. New results

This subsection examines the vibrational behavior of a relatively thick cracked nano-beam embedded in an elastic foundation. The length and thickness of the beam are assumed to be $L = 10$ nm and $h = 1$ nm, respectively (i.e. a beam aspect ratio of 10). The results are obtained for two boundary conditions, which are S-S and C-C, and the aspect ratio λ , nonlocal parameters ζ , foundation stiffnesses k_w and k_p ,

temperature parameter p_{th} , crack severity k^* , and crack location l_c are varied.

3.2.1. Effect of beam aspect ratio, nonlocal and temperature parameters

In this section, the effect of changing the beam aspect ratio and the nonlocal parameter on the beam fundamental natural frequency is considered. These cases are studied for three different dimensionless thermal loads (temperature parameter). The following range of study

Table 5
First four dimensionless frequencies $(\bar{\omega}_n)^2$ with $k_w = 10$, $k_p = 5$ and S-S boundary condition for different nonlocal parameters ζ .

ζ	$(\bar{\omega}_1)^2$			$(\bar{\omega}_2)^2$			$(\bar{\omega}_3)^2$			$(\bar{\omega}_4)^2$		
	a	b	c	a	b	c	a	b	c	a	b	c
0	12.5203	12.5146	12.5189	42.0231	42.0126	42.0005	91.3470	91.3260	91.2313	160.425	160.383	160.059
0.1	12.1658	12.1636	12.1646	36.3978	36.3884	36.3791	68.0635	68.0447	67.9812	102.314	102.285	102.091
0.2	11.3660	11.3636	11.3649	28.4900	28.4815	28.4767	46.7661	46.7512	46.7149	64.8678	64.8468	64.7402
0.3	10.5325	10.5297	10.5316	23.4457	23.4372	23.4359	36.4878	36.4738	36.4526	49.3844	49.3651	49.2987
0.4	9.85475	9.85130	9.85396	20.5039	20.4945	20.4963	31.1898	31.1748	31.1633	41.8205	41.8001	41.7567
0.5	9.35098	9.34680	9.35030	18.7291	18.7183	18.7229	28.1803	28.1633	28.1590	37.6247	37.6017	37.5739

a- Ref. [65], b- Ref. [16], c- Present results.

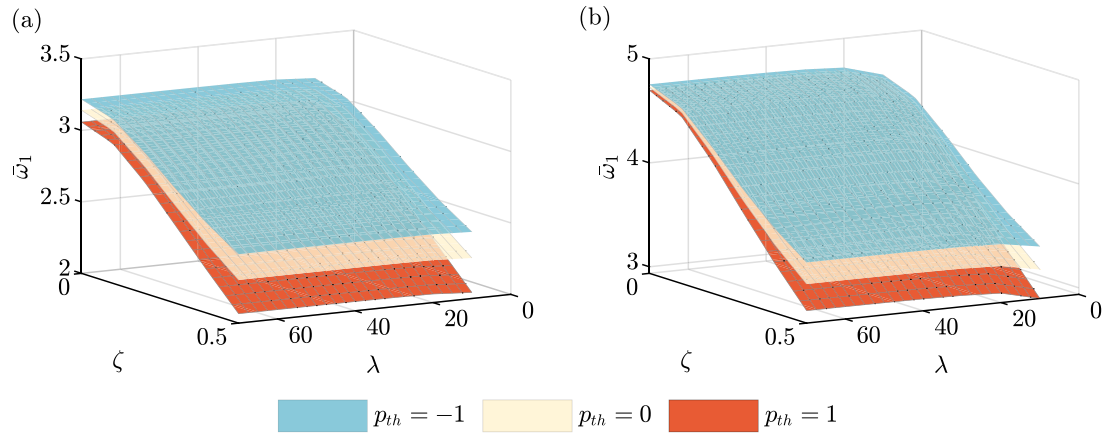


Fig. 4. (Color online) Dimensionless fundamental natural frequency $\bar{\omega}_1$ versus nonlocal parameter ζ and aspect ratio λ for three thermal parameter values p_{th} and (a) S-S and (b) C-C boundary conditions.

was selected; the beam aspect ratio $\lambda \in [20, 80]$ and the nonlocal parameter $\zeta \in [0, 0.5]$. Two boundary conditions are considered which are S-S and C-C as shown in Figs. 4(a) and 4(b) respectively. For each boundary condition, three temperature parameters $p_{th} \in \{-1, 0, 1\}$ are considered as shown in Fig. 4. The results show that increasing both the nonlocal and thermal parameters decreases the beam dimensionless natural frequency. Furthermore, increasing the aspect ratio increases the beam dimensionless natural frequency.

3.2.2. Effects of elastic foundation parameters versus the temperature parameter

In this section, similar analysis to the previous section is adopted to investigate the effect Winkler k_w and Pasternak k_p elastic foundation stiffness parameters on the dimensionless fundamental frequency. The ranges of the parameters are $k_w \in [0, 10]$ and $k_p \in [0, 10]$, as shown in Fig. 5. C-C and S-S boundary conditions are considered in Figs. 5(a) and 5(b) respectively. All the results are obtained at three different temperatures $p_{th} \in \{-1, 0, 1\}$. The results shown in Fig. 5 indicate that increasing the elastic foundation stiffness increases the dimensionless fundamental frequency. Moreover, the effect of changing the Pasternak foundation stiffness on the fundamental frequency is higher than that of the Winkler foundation. In addition, the effect of increasing the thermal parameter is to decrease the fundamental frequency which makes sense as increasing the temperature will increase the axial force for these boundary conditions. Subsequently, the fundamental frequency decreases.

3.2.3. Effects of crack severity k^* and crack location ratio l_c versus the thermal parameter

In this section the combined effect of crack location, crack severity and the thermal parameter are investigated. The first three natural frequencies are evaluated while changing the crack location in the range $l_c \in [0.05, 0.95]$. Two values of crack severity are considered, $k^* \in \{1, 2\}$, and two boundary conditions are considered. The results are plotted in Fig. 6, where the first row gives the S-S results and the

second row gives the C-C results. The first, second and third columns of the figure give the first, second and third natural frequencies. In each subfigure of Fig. 6 there are six plots which represent three different thermal loading parameters $p_{th} \in \{-2, 0, 2\}$ at two different crack severities. The vertical axis of all subfigures represents the frequency ratio $\bar{\omega}$.

The results of the figure indicate that increasing either or both the crack severity and thermal parameter decreases the frequency ratio. Also, along the beam length there are insensitive crack locations and sensitive crack locations which varies with the boundary condition and with vibration mode, as shown in Fig. 6. It is important to note that, the insensitive location is the crack location at which $\bar{\omega} \approx 1$ and the most sensitive location is the location of $\min(\bar{\omega})$.

In sub- Fig. 6(a1), which is the first mode for the S-S cracked beam, it can be seen that the dashed blue line goes to zero when $l_c \in [0.3, 0.7]$. This case occurs at conditions of a crack severity $k^* = 2$ and thermal dimensionless parameter $p_{th} = 2$. This phenomenon may be explained by the fact that both the crack and the axial load resulted from heating reduces the beam stiffness until the Hopf bifurcation point corresponding to the critical buckling load is reached. This case is further investigated in the next subsection.

3.2.4. Effects of crack location ratio and thermal parameter at several crack severities

In this section, the effects of crack location $l_c \in [0.05, 0.95]$ and the thermal parameter on the fundamental natural frequency are investigated. The investigation is performed for a S-S beam as shown Figs. 7(a1), 7(a2) and 7(a3) and for a C-C beam as shown in Figs. 7(b1), 7(b2) and 7(b3). Three different crack severities are considered, which are $k^* \in \{0, 2, 4\}$, which are shown in the first, second and third columns of Fig. 7 respectively. Fig. 7(a1) is obtained for the case of an uncracked simply supported nano-beam. The results show that at $p_{th} \approx \pi^2$, which corresponds to the critical buckling load, the fundamental frequency approaches zero. Fig. 7(a2) is for a cracked simply supported beam with crack severity $k^* = 2$, which shows that the lowest thermal

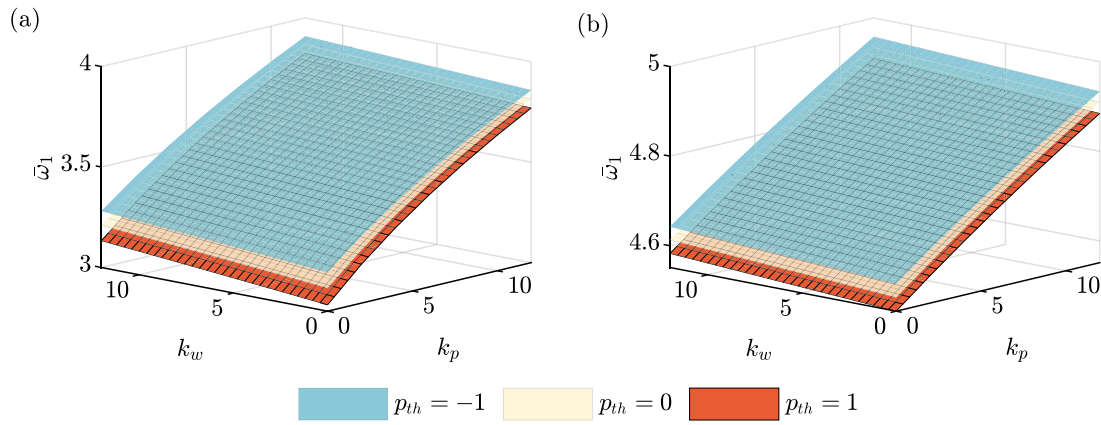


Fig. 5. (Color online) Dimensionless fundamental natural frequency $\bar{\omega}_1$ versus elastic foundation parameters (Winkler k_w and Pasternak k_p) for temperature parameter p_{th} and (a) S-S and (b) C-C boundary conditions.

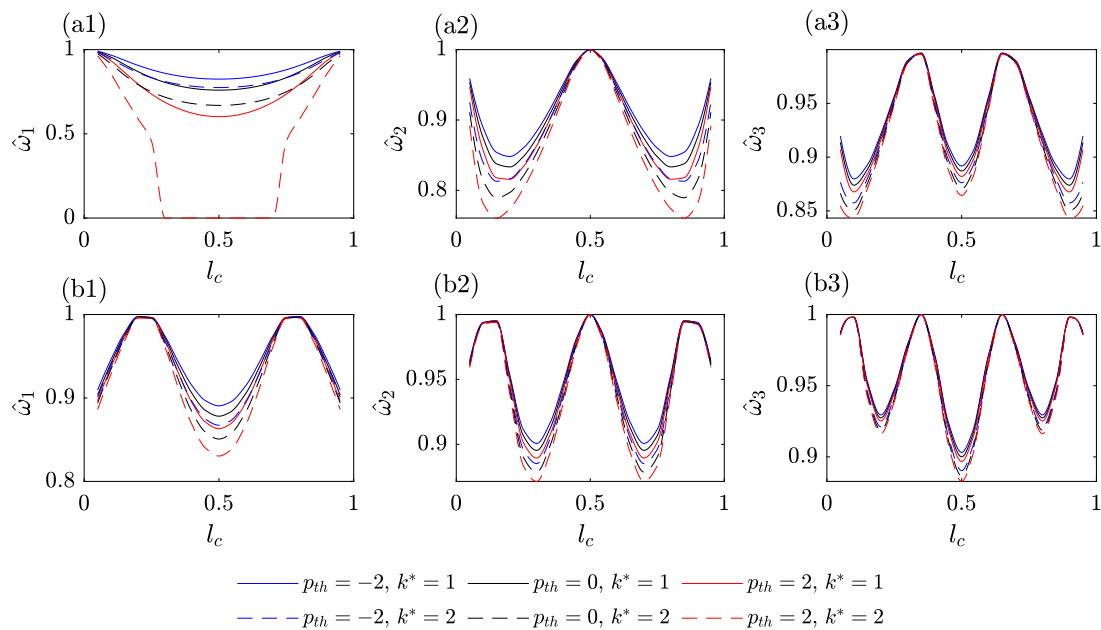


Fig. 6. (Color online) dimensionless first three natural frequencies ratio $\bar{\omega}_n$ versus crack location l_c for crack severity k^* and temperature parameter p_{th} of (a) S-S and (b) C-C boundary conditions.

dimensionless load required to reach the condition of zero fundamental frequency, i.e. the buckling load, occurs at $p_{th} \approx 2$ and $l_c \in [0.3, 0.7]$. This critical load value increases when the crack location is outside this range, i.e. $l_c \notin [0.3, 0.7]$. Further increases of the crack severity increases the range of crack location at which the critical thermal load occurs, i.e. $l_c \in [0.15, 0.85]$ in Fig. 7(a3) for $k^* = 4$.

The analysis for the case of a C-C beam shows similar behavior but at different values of critical thermal load. Theoretically, the critical buckling load for a C-C Euler beam is $p_{th} = 4 \times \pi^2$ and this explains why $\bar{\omega}_1 > 0$ in Fig. 7(b1) where the investigated range is $p_{th} \in [10, 20]$. However, with the increase of crack severity the critical thermal load is reached earlier, as shown in Figs. 7(b2) and 7(b3), with critical loads $p_{th} \approx 14$ and $p_{th} \approx 12$ respectively. The results in Fig. 7 demonstrate that the critical thermal load occurs earlier for S-S beams than for C-C beams.

3.2.5. Various crack severities, foundation stiffness, temperature parameter, and nonlocal parameter effects

In this section, the variations in dimensionless fundamental frequency $\bar{\omega}_1$ for both S-S and C-C beams with various temperature parameters p_{th} , foundation stiffnesses k_w and k_p , crack severities k^* ,

and nonlocal parameter ζ are listed in Table 6 for a crack located at $l_c = 0.5$. The results show that increasing the crack severity, nonlocal parameter or temperature parameter decreases the fundamental frequency. In addition, increasing the elastic foundation stiffness increases the fundamental frequency.

4. Conclusion

The study introduces a novel approach to investigate the thermal lateral vibration behavior of cracked nanobeams embedded on two distinct elastic foundations, using Reddy beam theory. This research contribution is significant for the field of nanostructures, as it provides valuable insights into the behavior of these nanostructures, which are crucial for designing and developing nanoscale devices. Furthermore, nonlocal elasticity theory is incorporated to account for the size effect of the nanostructure, which is an essential consideration in the analysis of such systems. Two rotational springs with stiffness corresponding to the crack severity were used to simulate the nanobeam's cracked section. This approach differs from traditional CBT and FSDT, where only one rotational spring was used to simulate the presence of a crack in bending vibration. Although the model is general, only the effect of

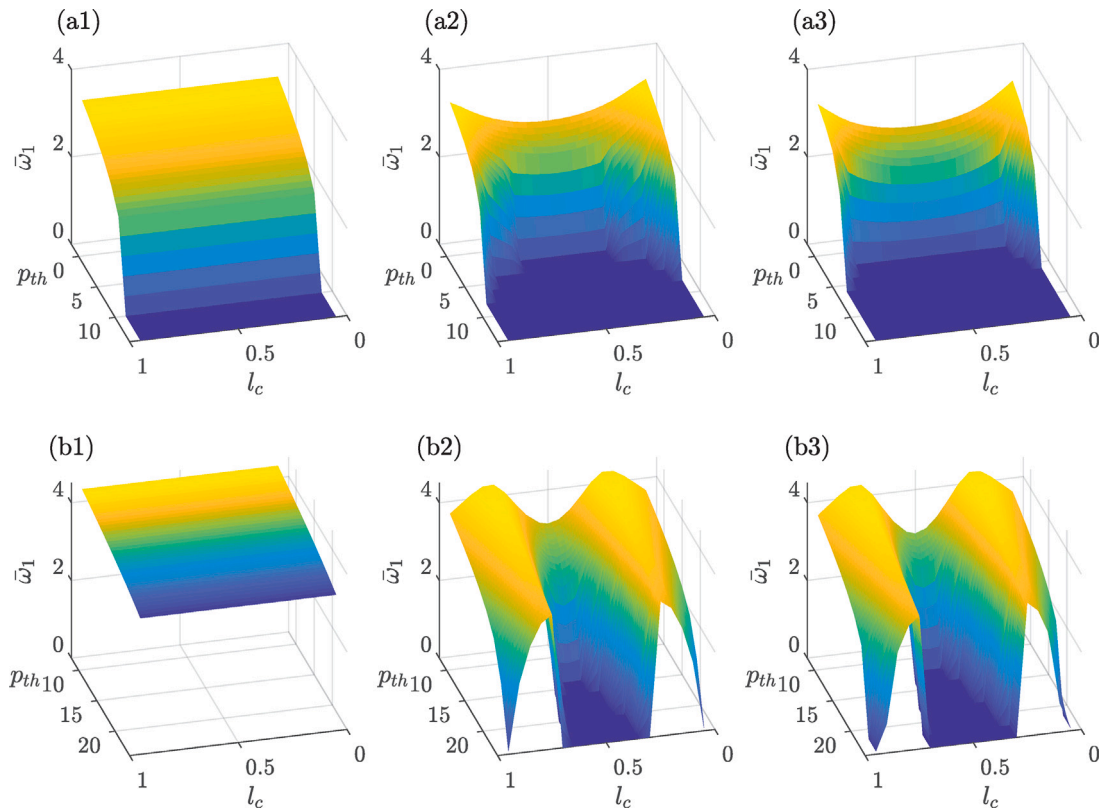


Fig. 7. (Color online) Dimensionless fundamental natural frequency $\bar{\omega}_1$ versus different crack location l_c and thermal parameter p_{th} for crack severity k^* for (a) S-S and (b) C-C boundary conditions, where (a1), (a2) and (a3) are for $k^* \in \{0, 2, 4\}$ and (b1), (b2) and (b3) are for $k^* \in \{0, 2, 4\}$ respectively.

Table 6
Dimensionless fundamental natural frequency $\bar{\omega}_1$ for different nonlocal parameters ζ , elastic foundation (k_w, k_p) , crack severity K^* and temperature parameter p_{th} for S-S and C-C boundary conditions.

S-S				C-C											
k^*	(k_w, k_p)	$\zeta = 0$			$\zeta = 0.2$			k^*	(k_w, k_p)	$\zeta = 0$			$\zeta = 0.2$		
		p_{th}			p_{th}					p_{th}			p_{th}		
		-1	0	1	-1	0	-1			-1	-1	0	-1	0	1
0	(0, 0)	3.194	3.116	3.031	2.966	2.867	2.757	0	(0, 0)	4.613	4.582	4.551	4.221	4.147	3.591
	(5, 5)	3.545	3.489	3.430	3.385	3.320	3.251	(5, 5)	4.767	4.739	4.712	4.552	4.494	4.434	
	(10, 5)	3.573	3.518	3.460	3.416	3.353	3.286	(10, 5)	4.778	4.751	4.723	4.565	4.508	4.448	
	(10, 10)	3.815	3.770	3.724	3.689	3.639	3.587	(10, 10)	4.906	4.881	4.856	4.823	4.775	4.725	
1	(0, 0)	2.546	2.366	2.130	2.338	2.163	1.957	1	(0, 0)	4.081	4.024	3.964	3.643	3.560	3.444
	(5, 5)	3.162	3.075	2.980	2.932	2.852	2.764	(5, 5)	4.342	4.297	4.251	4.001	3.941	3.879	
	(10, 5)	3.200	3.117	3.026	2.980	2.904	2.821	(10, 5)	4.357	4.313	4.267	4.020	3.961	3.900	
	(10, 10)	3.541	3.481	3.417	3.294	3.238	3.180	(10, 10)	4.556	4.519	4.480	4.280	4.232	4.182	
2	(0, 0)	2.340	2.084	1.666	2.139	1.901	1.528	2	(0, 0)	3.965	3.899	3.829	3.518	3.428	3.314
	(5, 5)	3.076	2.979	2.870	2.839	2.749	2.650	(5, 5)	4.260	4.210	4.158	3.906	3.842	3.774	
	(10, 5)	3.118	3.024	2.921	2.891	2.807	2.715	(10, 5)	4.276	4.227	4.175	3.926	3.863	3.797	
	(10, 10)	3.488	3.424	3.355	3.229	3.170	3.107	(10, 10)	4.494	4.454	4.412	4.202	4.151	4.099	
3	(0, 0)	2.231	1.917	1.209	2.036	1.746	1.114	3	(0, 0)	3.913	3.843	3.767	3.464	3.369	3.255
	(5, 5)	3.038	2.935	2.819	2.798	2.704	2.600	(5, 5)	4.225	4.172	4.118	3.867	3.800	3.731	
	(10, 5)	3.081	2.983	2.873	2.853	2.765	2.668	(10, 5)	4.241	4.189	4.135	3.888	3.823	3.754	
	(10, 10)	3.465	3.399	3.328	3.203	3.142	3.077	(10, 10)	4.468	4.427	4.383	4.171	4.119	4.065	

two boundary conditions, S-S and C-C, are considered. In addition, the influence of other important parameters such as the Winkler and Pasternak foundation stiffnesses, nonlocal parameter, aspect ratio, thermal effect, crack severity and crack location are investigated. The following crucial conclusions may be derived from the results:

- It is crucial to emphasize TSDT's advantage over FSDT in thick beam analysis is that the determination of a shear correction coefficient κ is not required.

- Insensitive and sensitive crack locations are dependent on the boundary conditions and vibration mode.

- A thermal parameter higher than zero acts as a compression load, which may cause buckling to the beam if it reaches the critical buckling load value.

- The presence of a crack reduces the critical thermal load parameter. This effect increases when the crack is located in a sensitive crack location.

The results obtained from this study are expected to provide a useful reference for future research on the thermal vibration behavior of cracked nanobeams.

Funding information

The authors declare that they do not receive any funds from any organization for this research.

CRedit authorship contribution statement

Moustafa S. Taima: Writing – original draft, Software, Formal analysis. **Tamer A. El-Sayed:** Writing – review & editing, Writing – original draft, Supervision, Conceptualization. **Michael I. Friswell:** Writing – review & editing, Validation, Supervision.

Declaration of competing interest

The authors declare that they have no known competing financial interests or personal relationships that could have appeared to influence the work reported in this paper.

Data availability

Data will be made available on request.

Appendix A. FE weak form

The weak form of Eq. (31) for the beam length from 0 to L can be obtained using traditional finite element (FE) techniques, resulting in Eq. (34). The first step involves multiplying Eq. (31) with the weight function V to obtain:

$$-EAVU'' - \rho A \omega^2 (VU - \mu VU'') = 0. \tag{A.1}$$

Integrating Eq. (A.1) over the length of the beam and using integration-by-parts, we obtain:

$$\int_0^L -EAVU'' - \rho A \omega^2 (VU - \mu VU'') dx = \int_0^L EAV'U' - \rho A \omega^2 (VU + \mu V'U') dx + [V(-EAU' + \mu \rho A \omega^2 U')]_0^L. \tag{A.2}$$

Appendix B. Elements of stiffness and mass matrix

The finite element stiffness and mass matrices may be written as

$$\begin{aligned} [K_e] &= EA \mathbf{x}_2 + K_w \mathbf{x}_3 + \left(\frac{8}{15}GA + K_p - EA\alpha\Delta T + \mu K_w\right) \mathbf{x}_4 \\ &+ \left(\frac{1}{21}EI + \mu(K_p - EA\alpha\Delta T)\right) \mathbf{x}_5 \\ &+ \frac{8}{15}GA \mathbf{x}_6 + \frac{68}{105}EI \mathbf{x}_7 + \frac{8}{15}GA (\mathbf{x}'_8 + \mathbf{x}_8) - \frac{16}{105}EI (\mathbf{x}'_9 + \mathbf{x}_9), \end{aligned} \tag{B.1}$$

and

$$\begin{aligned} [M_e] &= \rho A (\mathbf{x}_1 + \mu \mathbf{x}_2 + \mathbf{x}_3 + \mu \mathbf{x}_4) + \frac{1}{21} \rho I (\mathbf{x}_4 + \mu \mathbf{x}_5) \\ &+ \frac{68}{105} \rho I (\mathbf{x}_6 + \mu \mathbf{x}_7) - \frac{16}{105} \rho I (\mathbf{x}'_8 + \mathbf{x}_8 + \mu (\mathbf{x}'_9 + \mathbf{x}_9)), \end{aligned} \tag{B.2}$$

where

$$\mathbf{x}_1 = \int_0^L \mathbf{V}_i \mathbf{V}_j^T dx, \tag{B.3}$$

$$\mathbf{x}_2 = \int_0^L \mathbf{V}'_i \mathbf{V}'_j{}^T dx, \tag{B.4}$$

$$\mathbf{x}_3 = \int_0^L \mathbf{Y}_i \mathbf{Y}_j^T dx, \tag{B.5}$$

$$\mathbf{x}_4 = \int_0^L \mathbf{Y}'_i \mathbf{Y}'_j{}^T dx, \tag{B.6}$$

$$\mathbf{x}_5 = \int_0^L \mathbf{Y}''_i \mathbf{Y}''_j{}^T dx, \tag{B.7}$$

$$\mathbf{x}_6 = \int_0^L \Phi_i \Phi_j^T dx, \tag{B.8}$$

$$\mathbf{x}_7 = \int_0^L \Phi'_i \Phi'_j{}^T dx, \tag{B.9}$$

$$\mathbf{x}_8 = \int_0^L \Phi_i \mathbf{Y}_j^T dx, \tag{B.10}$$

$$\mathbf{x}_9 = \int_0^L \Phi'_i \mathbf{Y}'_j{}^T dx. \tag{B.11}$$

The stiffness and mass matrices and force vector are rearranged according to the displacement vector $\Delta_e = [u_1 \ w_1 \ \theta_1 \ \psi_1 \ u_2 \ w_2 \ \theta_2 \ \psi_2]^T$. The shape functions for a Reddy beam for generalized displacements \mathbf{V} , \mathbf{Y} and Φ are:

$$\mathbf{V}_i = \left[1 - \frac{x}{L}, 0, 0, 0, \frac{x}{L}, 0, 0, 0\right], \tag{B.12}$$

$$\begin{aligned} \mathbf{Y}_i &= \left[0, 1 - 3\left(\frac{x}{L}\right)^2 + 2\left(\frac{x}{L}\right)^3, x\left(1 - \frac{x}{L}\right)^2, 0, 0, 3\left(\frac{x}{L}\right)^2, \right. \\ &\quad \left. - 2\left(\frac{x}{L}\right)^3, x\left(\left(\frac{x}{L}\right)^2 - \frac{x}{L}\right), 0\right], \end{aligned} \tag{B.13}$$

$$\Phi_i = \left[0, 0, 0, 1 - \frac{x}{L}, 0, 0, 0, \frac{x}{L}\right]. \tag{B.14}$$

References

- [1] A. Kiani, M. Sheikhhoshkar, A. Jamalpoor, M. Khanzadi, Free vibration problem of embedded magneto-electro-thermo-elastic nanoplate made of functionally graded materials via nonlocal third-order shear deformation theory, *J. Intell. Mater. Syst. Struct.* 29 (5) (2018) 741–763, <http://dx.doi.org/10.1177/1045389x17721034>.
- [2] A.H. Lebaschi, X.-H. Deng, C.L. Camp, J. Zong, G.-T. Cong, C.B. Carballo, Z. Album, S.A. Rodeo, Biomechanical, histologic, and molecular evaluation of tendon healing in a new murine model of rotator cuff repair, *Arthrosc. J. Arthrosc. Relat. Surg.* 34 (4) (2018) 1173–1183, <http://dx.doi.org/10.1016/j.arthro.2017.10.045>.
- [3] K.L. Johnson, M.J. Gidley, A. Bacic, M.S. Doblin, Cell wall biomechanics: a tractable challenge in manipulating plant cell walls ‘fit for purpose’, *Curr. Opin. Biotechnol.* 49 (2018) 163–171, <http://dx.doi.org/10.1016/j.copbio.2017.08.013>.
- [4] T. Murmu, S. Adhikari, Nonlocal frequency analysis of nanoscale biosensors, *Sensors Actuators A* 173 (1) (2012) 41–48, <http://dx.doi.org/10.1016/j.sna.2011.10.012>.
- [5] B. Akgöz, Ö. Civalek, Buckling analysis of functionally graded tapered microbeams via Rayleigh-Ritz method, *Mathematics* 10 (23) (2022) <http://dx.doi.org/10.3390/math10234429>.
- [6] S. Yin, Z. Xiao, Y. Deng, G. Zhang, J. Liu, S. Gu, Isogeometric analysis of size-dependent Bernoulli–Euler beam based on a reformulated strain gradient elasticity theory, *Comput. Struct.* 253 (2021) 106577, <http://dx.doi.org/10.1016/j.compstruc.2021.106577>.
- [7] M.H. Jalaei, H.T. Thai, Ö. Civalek, On viscoelastic transient response of magnetically imperfect functionally graded nanobeams, *Internat. J. Engrg. Sci.* 172 (2022) 103629, <http://dx.doi.org/10.1016/j.ijengsci.2022.103629>.
- [8] S. Ceballes, K. Larkin, E. Rojas, S.S. Ghaffari, A. Abdelkefi, Nonlocal elasticity and boundary condition paradoxes: a review, *J. Nanoparticle Res.* 23 (3) (2021) 66, <http://dx.doi.org/10.1007/s11051-020-05107-y>.
- [9] S. Gopalakrishnan, S. Narendar, *Wave Propagation in Nanostructures: Nonlocal Continuum Mechanics Formulations*, Springer Science & Business Media, 2013.
- [10] M.A. Eltahir, N.A. Mohamed, Vibration of nonlocal perforated nanobeams with general boundary conditions, *Smart Struct. Syst.* 25 (4) (2020) 501–514, <http://dx.doi.org/10.12989/ss.2020.25.4.501>.
- [11] M.S. Taima, T.A. El-Sayed, S.H. Farghaly, Free vibration analysis of multistep nonlocal Bernoulli–Euler beams using dynamic stiffness matrix method, *J. Vib. Control* 27 (7–8) (2020) 774–789, <http://dx.doi.org/10.1177/1077546320933470>.
- [12] M.S. Taima, T. El-Sayed, S.H. Farghaly, Longitudinal vibration analysis of a stepped nonlocal rod embedded in several elastic media, *J. Vib. Eng. Technol.* 10 (4) (2022) 1399–1412, <http://dx.doi.org/10.1007/s42417-022-00454-7>.

- [13] J.N. Reddy, Nonlocal theories for bending, buckling and vibration of beams, *Internat. J. Engrg. Sci.* 45 (2) (2007) 288–307, <http://dx.doi.org/10.1016/j.ijengsci.2007.04.004>.
- [14] M. Aydogdu, A general nonlocal beam theory: its application to nanobeam bending, buckling and vibration, *Physica E* 41 (9) (2009) 1651–1655.
- [15] I. Mechab, N. El Meiche, F. Bernard, Free vibration analysis of higher-order shear elasticity nanocomposite beams with consideration of nonlocal elasticity and Poisson effect, *J. Nanomech. Micromech.* 6 (3) (2016) 04016006, [http://dx.doi.org/10.1061/\(ASCE\)NM.2153-5477.0000110](http://dx.doi.org/10.1061/(ASCE)NM.2153-5477.0000110).
- [16] A.I. Aria, M.I. Friswell, T. Rabczuk, Thermal vibration analysis of cracked nanobeams embedded in an elastic matrix using finite element analysis, *Compos. Struct.* 212 (2019) 118–128, <http://dx.doi.org/10.1016/j.compstruct.2019.01.040>.
- [17] S. Ghannadpour, B. Mohammadi, J. Fazilati, Bending, buckling and vibration problems of nonlocal Euler beams using Ritz method, *Compos. Struct.* 96 (2013) 584–589, <http://dx.doi.org/10.1016/j.compstruct.2012.08.024>.
- [18] J. Kaplunov, D. Prikazchikov, L. Prikazchikova, On integral and differential formulations in nonlocal elasticity, *Eur. J. Mech. A Solids* (2022) 104497, <http://dx.doi.org/10.1016/j.euromechsol.2021.104497>.
- [19] H. Darban, F. Fabbrocino, L. Feo, R. Luciano, Size-dependent buckling analysis of nanobeams resting on two-parameter elastic foundation through stress-driven nonlocal elasticity model, *Mech. Adv. Mater. Struct.* 28 (23) (2021) 2408–2416, <http://dx.doi.org/10.1080/15376494.2020.1739357>.
- [20] A.A. Pisano, P. Fuschì, C. Polizzotto, Integral and differential approaches to Eringen's nonlocal elasticity models accounting for boundary effects with applications to beams in bending, 101 (8), 2021, e202000152, <http://dx.doi.org/10.1002/zamm.202000152>.
- [21] J. Fernández-Sáez, R. Zaera, J. Loya, J. Reddy, Bending of Euler–Bernoulli beams using Eringen's integral formulation: A paradox resolved, *Internat. J. Engrg. Sci.* 99 (2016) 107–116, <http://dx.doi.org/10.1016/j.ijengsci.2015.10.013>.
- [22] G. Romano, R. Barretta, M. Diaco, F. Marotti de Sciarra, Constitutive boundary conditions and paradoxes in nonlocal elastic nanobeams, *Int. J. Mech. Sci.* 121 (2017) 151–156, <http://dx.doi.org/10.1016/j.ijmecsci.2016.10.036>.
- [23] G.P. Lignola, F. Russo Spena, A. Prota, G. Manfredi, Exact stiffness–matrix of two nodes Timoshenko beam on elastic medium. An analogy with Eringen model of nonlocal Euler–Bernoulli nanobeams, *Comput. Struct.* 182 (2017) 556–572, <http://dx.doi.org/10.1016/j.compstruct.2016.12.003>.
- [24] A.C. Eringen, On differential equations of nonlocal elasticity and solutions of screw dislocation and surface waves, *J. Appl. Phys.* 54 (9) (1983) 4703–4710.
- [25] G. Romano, R. Barretta, Nonlocal elasticity in nanobeams: the stress-driven integral model, *Internat. J. Engrg. Sci.* 115 (2017) 14–27, <http://dx.doi.org/10.1016/j.ijengsci.2017.03.002>.
- [26] G. Romano, R. Barretta, Stress-driven versus strain-driven nonlocal integral model for elastic nano-beams, *Composites B* 114 (2017) 184–188, <http://dx.doi.org/10.1016/j.compositesb.2017.01.008>.
- [27] M.Z. Salim, T.A. El-Sayed, E.M. Rabeih, S.H. Farghaly, Free vibration analysis for a pipe conveying fluid with intermediate support and carrying multiple concentrated masses, *Eng. Res. J.* 160 (2018) 26–43, <http://dx.doi.org/10.21608/erj.2018.139535>.
- [28] T.A. El-Sayed, H.H. El-Mongy, Application of variational iteration method to free vibration analysis of a tapered beam mounted on two-degree of freedom subsystems, *Appl. Math. Model.* 58 (2018) 349–364, <http://dx.doi.org/10.1016/j.apm.2018.02.005>.
- [29] S.P. Timoshenko, LXVI. On the correction for shear of the differential equation for transverse vibrations of prismatic bars, *Lond. Edinb. Dublin Philos. Mag. J. Sci.* 41 (245) (1921) 744–746, <http://dx.doi.org/10.1080/14786442108636264>.
- [30] T.A. El-Sayed, S.H. Farghaly, Formulae for the frequency equations of beam-column system carrying a fluid storage tank, *Struct. Eng. Mech.* 73 (1) (2020) 83–95, <http://dx.doi.org/10.12989/sem.2020.73.1.083>.
- [31] A. Elsawaf, T.A. Elsayed, S.H. Farghaly, Optimal Design for Maximum Fundamental Frequency and Minimum Intermediate Support Stiffness for Uniform and Stepped Beams Composed of Different Materials, *SAE International*, 2020, <http://dx.doi.org/10.4271/2020-01-5014>.
- [32] T.A. El-Sayed, H.H. El-Mongy, A new numeric–symbolic procedure for variational iteration method with application to the free vibration of generalized multi-span Timoshenko beam, *J. Vib. Control* 28 (7–8) (2022) 799–811, <http://dx.doi.org/10.1177/1077546320983192>.
- [33] T.A. El-Sayed, S.H. Farghaly, Frequency equation using new set of fundamental solutions with application on the free vibration of Timoshenko beams with intermediate rigid or elastic span, *J. Vib. Control* 24 (20) (2018) 4764–4780, <http://dx.doi.org/10.1177/1077546317734102>.
- [34] T.A. El-Sayed, S.H. Farghaly, A normalized transfer matrix method for the free vibration of stepped beams: Comparison with experimental and FE(3D) methods, *Shock Vib.* 2017 (2017) 8186976, <http://dx.doi.org/10.1155/2017/8186976>.
- [35] S.H. Farghaly, T.A. El-Sayed, Exact free vibration of multi-step Timoshenko beam system with several attachments, *Mech. Syst. Signal Process.* 72–73 (2016) 525–546, <http://dx.doi.org/10.1016/j.ymsp.2015.11.025>.
- [36] T.A. El-Sayed, S.H. Farghaly, Exact vibration of Timoshenko beam combined with multiple mass spring sub-systems, *Struct. Eng. Mech.* 57 (6) (2016) 989–1014, <http://dx.doi.org/10.12989/sem.2016.57.6.989>.
- [37] S.H. Farghaly, T.A. El-Sayed, Exact free vibration analysis for mechanical system composed of Timoshenko beams with intermediate eccentric rigid body on elastic supports: An experimental and analytical investigation, *Mech. Syst. Signal Process.* 82 (2017) 376–393, <http://dx.doi.org/10.1016/j.ymsp.2016.05.029>.
- [38] M. Salamat-Talab, A. Nateghi, J. Torabi, Static and dynamic analysis of third-order shear deformation FG micro beam based on modified couple stress theory, *Int. J. Mech. Sci.* 57 (1) (2012) 63–73.
- [39] F. Lin, Y. Xiang, Vibration of carbon nanotube reinforced composite beams based on the first and third order beam theories, *Appl. Math. Model.* 38 (15–16) (2014) 3741–3754.
- [40] R. Ansari, E. Hasrati, R. Gholami, F. Sadeghi, Nonlinear analysis of forced vibration of nonlocal third-order shear deformable beam model of magneto–electro–thermo elastic nanobeams, *Composites B* 83 (2015) 226–241, <http://dx.doi.org/10.1016/j.compositesb.2015.08.038>.
- [41] F. Ebrahimi, M.R. Barati, A nonlocal higher-order shear deformation beam theory for vibration analysis of size-dependent functionally graded nanobeams, *Arab. J. Sci. Eng.* 41 (5) (2016) 1679–1690.
- [42] F. Lin, L.H. Tong, H.S. Shen, C.W. Lim, Y. Xiang, Assessment of first and third order shear deformation beam theories for the buckling and vibration analysis of nanobeams incorporating surface stress effects, *Int. J. Mech. Sci.* 186 (2020) 105873, <http://dx.doi.org/10.1016/j.ijmecsci.2020.105873>.
- [43] K. Sharma, K.K. Saxena, M. Shukla, Effect of multiple stone-Wales and vacancy defects on the mechanical behavior of carbon nanotubes using molecular dynamics, *Procedia Eng.* 38 (2012) 3373–3380, <http://dx.doi.org/10.1016/j.proeng.2012.06.390>, International conference on modelling optimization and computing.
- [44] S. Guler, Free vibration analysis of a rotating single edge cracked axially functionally graded beam for flap-wise and chord-wise modes, *Eng. Struct.* 242 (2021) 112564, <http://dx.doi.org/10.1016/j.engstruct.2021.112564>, URL <https://www.sciencedirect.com/science/article/pii/S0141029621000961>.
- [45] M. De Rosa, M. Lippiello, Closed-form solutions for vibrations analysis of cracked Timoshenko beams on elastic medium: An analytically approach, *Eng. Struct.* 236 (2021) 111946, <http://dx.doi.org/10.1016/j.engstruct.2021.111946>, URL <https://www.sciencedirect.com/science/article/pii/S0141029621000961>.
- [46] I. Talebinejad, C. Fischer, F. Ansari, Numerical evaluation of vibration-based methods for damage assessment of cable-stayed bridges, *Comput.-Aided Civ. Infrastruct. Eng.* 26 (3) (2011) 239–251, <http://dx.doi.org/10.1111/j.1467-8667.2010.00684.x>.
- [47] T. Van Do, D.H. Doan, N.D. Duc, T.Q. Bui, Phase-field thermal buckling analysis for cracked functionally graded composite plates considering neutral surface, *Compos. Struct.* 182 (2017) 542–548, <http://dx.doi.org/10.1016/j.compstruct.2017.09.059>.
- [48] P.P. Minh, N.D. Duc, The effect of cracks and thermal environment on free vibration of FGM plates, *Thin-Walled Struct.* 159 (2021) 107291, <http://dx.doi.org/10.1016/j.tws.2020.107291>.
- [49] P.P. Minh, D.T. Manh, N.D. Duc, Free vibration of cracked FGM plates with variable thickness resting on elastic foundations, *Thin-Walled Struct.* 161 (2021) 107425, <http://dx.doi.org/10.1016/j.tws.2020.107425>.
- [50] D.H. Doan, T.V. Do, P.M. Pham, N.D. Duc, Validation simulation for free vibration and buckling of cracked Mindlin plates using phase-field method, *Mech. Adv. Mater. Struct.* 26 (12) (2019) 1018–1027, <http://dx.doi.org/10.1080/15376494.2018.1430262>.
- [51] R. Nazemnezhad, P. Fahimi, Free torsional vibration of cracked nanobeams incorporating surface energy effects, *Appl. Math. Mech.* 38 (2) (2017) 217–230.
- [52] Ş.D. Akbaş, Forced vibration analysis of cracked nanobeams, *J. Braz. Soc. Mech. Sci. Eng.* 40 (8) (2018) 392, <http://dx.doi.org/10.1007/s40430-018-1315-1>.
- [53] Ş.D. Akbaş, M. ÖzgürYaylı, B. Deliktaş, B. Uzun, Vibration analysis of cracked microbeams by using finite element method, in: G.Z. Voyiadjis (Ed.), *Handbook of Damage Mechanics: Nano to Macro Scale for Materials and Structures*, Springer New York, New York, NY, 2020, pp. 1–12, http://dx.doi.org/10.1007/978-1-4614-8968-9_88-1.
- [54] T.A. El-Sayed, S.H. Farghaly, Exact free vibration analysis of Timoshenko stepped shaft carrying elastically supported eccentric masses with application on SWRO mechanical system, *Desalination* 385 (2016) 194–206.
- [55] J. Loya, J. Aranda-Ruiz, R. Zaera, Natural frequencies of vibration in cracked Timoshenko beams within an elastic medium, *Theor. Appl. Fract. Mech.* 118 (2022) 103257, <http://dx.doi.org/10.1016/j.tafmec.2022.103257>.
- [56] F. Ebrahimi, E. Salari, Effect of various thermal loadings on buckling and vibrational characteristics of nonlocal temperature-dependent functionally graded nanobeams, *Mech. Adv. Mater. Struct.* 23 (12) (2016) 1379–1397, <http://dx.doi.org/10.1080/15376494.2015.1091524>.
- [57] L.-L. Ke, Y.-S. Wang, Z.-D. Wang, Thermal effect on free vibration and buckling of size-dependent microbeams, *Physica E* 43 (7) (2011) 1387–1393, <http://dx.doi.org/10.1016/j.physe.2011.03.009>.
- [58] A. Benzair, A. Tounsi, A. Besseghier, H. Heireche, N. Moulay, L. Boumia, The thermal effect on vibration of single-walled carbon nanotubes using nonlocal Timoshenko beam theory, *J. Phys. D: Appl. Phys.* 41 (22) (2008) 225404, <http://dx.doi.org/10.1088/0022-3727/41/22/225404>.
- [59] J.-C. Hsu, R.-P. Chang, W.-J. Chang, Resonance frequency of chiral single-walled carbon nanotubes using Timoshenko beam theory, *Phys. Lett. A* 372 (16) (2008) 2757–2759, <http://dx.doi.org/10.1016/j.physleta.2008.01.007>.

- [60] Ç. Demir, Ö. Civalek, A new nonlocal FEM via hermitian cubic shape functions for thermal vibration of nano beams surrounded by an elastic matrix, *Compos. Struct.* 168 (2017) 872–884, <http://dx.doi.org/10.1016/j.compstruct.2017.02.091>.
- [61] A.C. Eringen, Nonlocal polar elastic continua, *Internat. J. Engrg. Sci.* 10 (1) (1972) 1–16, [http://dx.doi.org/10.1016/0020-7225\(72\)90070-5](http://dx.doi.org/10.1016/0020-7225(72)90070-5).
- [62] R. Barretta, R. Luciano, F. Marotti de Sciarra, G. Ruta, Stress-driven nonlocal integral model for Timoshenko elastic nano-beams, *Eur. J. Mech. A Solids* 72 (2018) 275–286, <http://dx.doi.org/10.1016/j.euromechsol.2018.04.012>.
- [63] A. Labib, D. Kennedy, C. Featherston, Free vibration analysis of beams and frames with multiple cracks for damage detection, *J. Sound Vib.* 333 (20) (2014) 4991–5003, <http://dx.doi.org/10.1016/j.jsv.2014.05.015>.
- [64] M.S. Taima, T. El-Sayed, M.B. Shehab, S.H. Farghaly, R.J. Hand, Vibration analysis of cracked beam based on reddy beam theory by finite element method, *J. Vib. Control* (2022) 10775463221122122, <http://dx.doi.org/10.1177/10775463221122122>.
- [65] N. Togun, S.M. Bağdatlı, Nonlinear vibration of a nanobeam on a pasternak elastic foundation based on non-local Euler-Bernoulli beam theory, *Math. Comput. Appl.* 21 (1) (2016) 3, URL <https://www.mdpi.com/2297-8747/21/1/3>.